Bioprinting 21 (2021) e00120

Contents lists available at ScienceDirect

Bioprinting

journal homepage: www.elsevier.com/locate/bprint

Advances in 3D bioprinting for the biofabrication of tumor models

Mónica Gabriela Sánchez-Salazar [a,b], Mario Moisés Álvarez [a,b,**], G. Trujillo-de Santiago [a,c,*]

[a] Centro de Biotecnología-FEMSA, Tecnologico de Monterrey, Monterrey, Nuevo Leon CP, 64849, Mexico
[b] Departamento de Bioingeniería, Tecnologico de Monterrey, Monterrey, Nuevo Leon CP, 64849, Mexico
[c] Departamento de Mecatrónica e Ingeniería Eléctrica, Tecnologico de Monterrey, Monterrey, Nuevo Leon CP, 64849, Mexico

ARTICLE INFO

Keywords:
3D bioprinting
Tumor complexity
Biofabrication
Vascularized tumor
Tissue engineering
Cancer modeling

ABSTRACT

Cancer research depends on the challenging task of producing representative and reliable models of human disease; these have largely been limited to mouse models or human cancer cell lines cultured in monolayers. Three-dimensional (3D) cell culture offers more realistic options, but conventional 3D models still fail to recreate the human tumor microenvironment. One biofabrication technique that has emerged as a powerful tool is 3D bioprinting, which can generate tumor constructs with increasing complexity. By incorporating factors like stromal cells, vasculature, hydrogels, and functional molecules into the bioprinting process, researchers are now able to create human tumor models that quite realistically represent human glioblastoma, breast, cervical, ovarian, hepatoma, lung, colon, and oral cancers. The obtained structures range from coaxially extruded fibers and monolayered grids to cylinders, cubes, discs, beads, and even mini-organs. Here, we discuss recent advances in cancer research based on 3D bioprinting. Our aim is to provide a broad perspective of the possibilities provided by this biofabrication technique for the generation of complex tumor models. We also review the different structures and characterization techniques used with these models. The use of 3D bioprinted tumors is increasing in areas like tumor biology, migration, invasion, and metastasis, as well as in pharmaceutical testing and even personalized medicine. Future work will involve improvement of the mechanical properties and chemical cues provided to the cells within the 3D constructs. The inclusion of several cell types within a single construct will upgrade current recapitulations of real tumor tissues. Bioprinting of cells cultured from patients' own biopsies will generate personalized models of the tumor niche.

1. Introduction

Cancer research depends on the availability of truly representative and reliable *in vitro* and *in vivo* disease models. However, the multifactorial nature of cancer as a disease makes this research difficult, expensive, and in need of a wide portfolio of resources [1]. In recent decades, our understanding of the molecular and genetic aspects of cancer has improved greatly. Knowledge of the cancer cell microenvironment and tumor heterogeneity has advanced significantly, but the complexity of *in vitro* tumor models still needs similar advances [2]. Many questions remain regarding key aspects of the tumor physiology, such as dormancy, indolent disease, relapse, metastatic colonization, and the rapid evolution of drug resistance.

The creation of realistic tumor models first requires the natural tumor microenvironment (TME) to be understood (Fig. 1). The TME of a given tumor reflects the various cell types, extracellular matrix (ECM), signaling molecules, and vasculature present within that tumor. More particularly, the cells within the TME include more than just cancer cells, as mesenchymal stem cells (MSCs), stromal cells, endothelial cells, and immune cells are also present [3,4].

The stromal cells are mostly represented by fibroblasts in various types of cancer. During the early tumor stages, they inhibit tumor progression [5]; however, they can later be modulated by the tumor cells and become transformed into cancer-associated fibroblasts (CAFs) [6]. The CAFs, as well as macrophages and endothelial cells, secrete numerous signaling molecules, such as vascular endothelial growth factor (VEGF), basic fibroblast growth factor (bFGF), transforming growth factor (TGF-α/β), epidermal growth factor (EGF), interleukin 1β (IL-1β), and other chemokines. These signaling molecules promote various cancer-related processes, including the epithelial-to-mesenchymal transition (EMT), tumor growth and angiogenesis, cancer cell migration, and tumor metastasis [7].

* Corresponding author. Centro de Biotecnología-FEMSA, Tecnológico de Monterrey, Monterrey, Nuevo León CP, 64849, México.
** Corresponding author. Centro de Biotecnología-FEMSA, Tecnológico de Monterrey, Monterrey, Nuevo León CP, 64849, México.
E-mail addresses: mario.alvarez@tec.mx (M.M. Álvarez), grissel@tec.mx (G. Trujillo-de Santiago).

https://doi.org/10.1016/j.bprint.2020.e00120
Received 15 June 2020; Received in revised form 5 December 2020; Accepted 7 December 2020

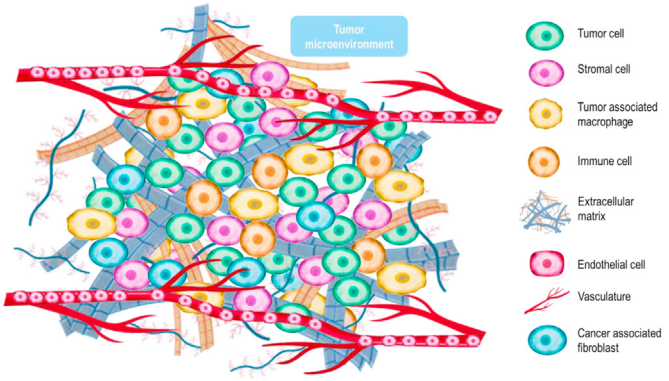

Fig. 1. The tumor microenvironment. Besides tumor cells, the ecosystem within and surrounding the tumor encompasses stromal cells (e.g., fibroblasts and adipocytes), tumor associated macrophages, cancer-associated fibroblasts, and immune cells, as well as the extracellular matrix (ECM) and vasculature.

The ECM is a vast array of molecular components with a tissue-specific composition that significantly affects cell phenotype and behavior [4,8,9]. In tumors, the ECM also can determine the cancer drug response [10–12]. The ECM consists of matrix proteins, glycoproteins, glycosaminoglycans, proteoglycans, growth factors, and other proteins [3,8,9].

Tumor vascularization is triggered by several different mechanisms, including sprouting angiogenesis, intussusceptive angiogenesis, recruitment of endothelial progenitor cells, vessel co-option, vasculogenic mimicry, and lymphangiogenesis [13].

Most cancer studies are performed in either 2D cell cultures [14,15] or in murine models [16–19]. The use of 2D cell culture has the advantage of studying human cancer cells; however, it entirely fails to recapitulate the TME due to the lack of 3D structure. Consequently, the cells undergo changes in gene and protein expression that are unique to cells cultured in monolayer and do not necessarily reflect gene expression in the tumors from which they were derived. Murine (or any other animal) models retain the advantages of being fully 3D and having the complexity of a natural tumor, but they are not 100% representative of human cancer physiology [20–22]. Furthermore, their use raises ethical concerns [23].

The limitations of these platforms raises the need for more representative 3D models that recapitulate human cancer cell morphology and tumor architecture and that more closely reflect the spontaneous cell differentiation, functional angiogenesis, and links between structure and function found in human tumors [24]. Current 3D models now allow pharmaceutical testing [2] and explorations of cancer biology [25] and immune oncology [26]. The present 3D cell culture platforms can be classified into scaffold associated (cells embedded in scaffolds) and scaffold-independent (spheroids [27] or organoids [28]) types. They can also be fabricated in specialized platforms, such as micropatterned plates and microfluidic systems [27].

One of the best examples of relevant 3D cancer models is the organoid, which is capable of mimicking the physiology, structure, dynamics, and functional aspects of its *in vivo* counterpart organ [29]. Organoids have now been generated from diverse human cancers, including breast, prostate, colon, pancreas, liver, and bladder cancers [30]. The generation of these complex cancer models has also been relevant for personalized or precision medicine applications [31], as molecular-targeting therapeutics may improve the outcome of cancer in patients. Nevertheless, the intratumoral and tumor heterogeneity among individual patients still challenges the efficacy of these therapeutics [32].

Tumor models and organoids, created at the micrometer scale, are now being used successfully to recapitulate the TME and to perform clinically relevant and personalized drug screening [33]. Similarly, tumor models sized in the millimeter range have been successfully used to mimic the TME, including its complement of stromal, endothelial, and cancer cells [34]. These micro- to millimeter sized tumor models are clinically relevant and have been remarkable facilitators of cancer research in recent years.

Having said that, the fabrication of larger, multi-cell type and vascularized (when relevant) tumors will further propel cancer research by enabling a more realistic recapitulation of the tumor microenvironment. Arguably, large and vascularized tumors are more frequently found in medical practice than are small and avascular tumors, and human tumors are typically only detected and treated when they exceed the millimeter range [35]. Vascularization is another frequent and clinical feature of actual tumors and is especially relevant because anti-cancer drugs are typically administered intravenously. Therefore, these drugs are transported to the tumor niche by convection (in circulating blood) through the tumor vascularization, followed by diffusion within the tumor and neighboring tissues. Accurately modeling the combined effect of convective and diffusive transport to tumor tissues will therefore require the fabrication of larger and vascularized models. At present, one of the main limitations that hinders the assembly and culture of tumor models larger than a few millimeters in size is the difficulty of developing vasculature [36]. The lack of vasculature in models larger than 400 μm results in the formation of a necrotic core—a feature that is actually common in real tumors at some developmental stages [36]. However, a vascular system is vital for the transport of nutrients and oxygen necessary to maintain cell viability and metabolic functions of larger tumors and to prevent extensive necrosis [37]. Oxygen and nutrient transport in tissues is limited to a diffusion distance of about 200 μm [38], so a growing tumor needs a vascular network to sustain its viability.

The introduction of 3D bioprinting is now allowing new opportunities to produce complex and vascularized tumor models. The 3D bioprinting process is a biofabrication technique that works by layer-by-layer construction of 3D tissues and biological constructs and can render hierarchical architectures similar to those of native tissues [39,40]. This technology, combined with biomaterial engineering and cell culture, allows an improved recapitulation of cancer tumors with an upgraded structure. The 3D bioprinting techniques can be distinguished by the main strategy used for printing and can include nozzle-based techniques (e.g., inkjet and extrusion, Fig. 2A and B), laser-based techniques (e.g., laser-assisted and stereolithography [SLA]/digital light processing [DLP]-based, Fig. 2D and E), and magnetic bioprinting (Fig. 2C) [41–43]. Magnetic bioprinting is a recently coined term and its use is still controversial. Several recent papers consider it to represent a bioprinting technique because the use of magnetic micro- or nanoparticles allows the precise deposition of cells into predesigned shapes, such as rings, dots, or spheroids [44–46]. However, the main difference between magnetic bioprinting and traditional bioprinting techniques are how bioinks are spatially arranged. Most bioprinting techniques deposit materials on a surface or project a light source to sculpt a predesigned shape. By contrast, magnetic bioprinting arranges the cells into specific shapes using magnetism. In the most commonly used embodiment of magnetic bioprinting, cells are loaded with magnetic nanoparticles, and magnets are used to control the rate and location of deposition of these cells [47] (Fig. 2C). This enables the assembly of cell tissue-like structures, due to the endogenous synthesis of ECM, without the need of encapsulating cells in a matrix substrate.

Despite this variety, the most common bioprinting technique continues to be extrusion due to its simplicity, low cost, minimal cell damage, and versatility, its ability to provide direct cell incorporation and homogeneous distribution, and the wider range of printable biomaterials available for extrusion [48].

The aim of this review is to explore the scope, limitations, and perspectives of 3D bioprinting as applied to the biofabrication of tumor models of different types of solid cancers. We will first analyze the strategies commonly used for characterization of inks and bioinks. We will then review the different structures employed and the characterization methods for the generated 3D constructs. We will also evaluate the complexity of various tumor models according to the different cell

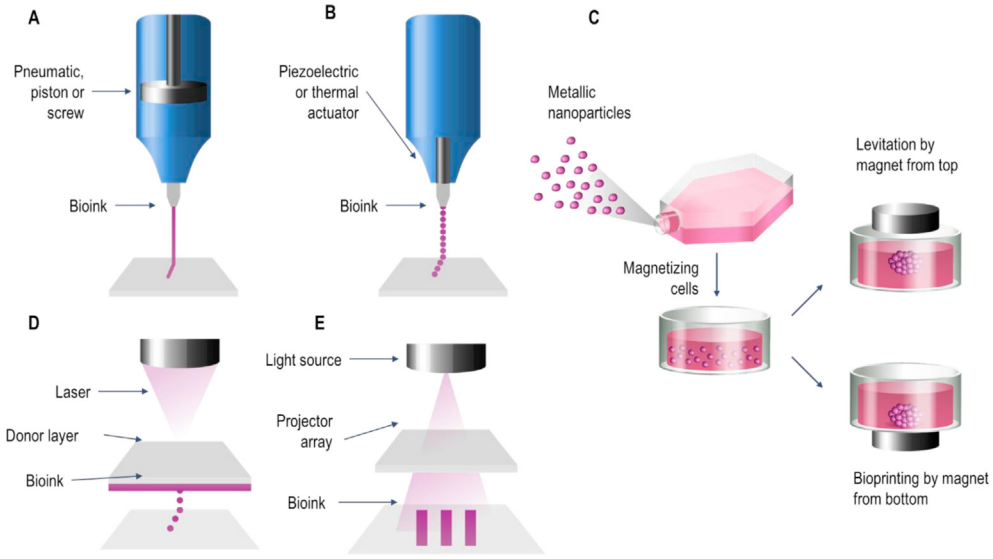

Fig. 2. Three-dimensional (3D) bioprinting platforms. (A) Extrusion creates filaments by pushing a bioink through the nozzle either by pneumatic, piston, or screw pressure. (B) Inkjet bioprinting consists of bioinks deposited into a desired pattern using droplets that are ejected via thermal or piezoelectric processes. (C) Magnetic levitation or bioprinting consists of magnetizing cells using metallic nanoparticles and then applying a magnet (either from the top or bottom) to create a structure. (D) Laser-assisted bioprinting is based on laser-induced forward-transfer, where a pulsed laser induces the transfer of material from a source film. (E) Stereolithography/Digital Light Processing uses UV or visible light to create patterns with photosensitive polymers in a layer-by-layer fashion.

types printed within a single construct. Finally, we will review the main applications of these models and the future perspectives of 3D bioprinting in cancer research (Fig. 3).

2. Key components for recapitulation of the tumor microenvironment

Recapitulation of the TME requires the inclusion of as many factors as possible that are typically present in that environment. It is also essential to consider the complexity of the extracellular matrix (ECM), the coexistence of tumor and stromal cells, and the presence of vasculature.

Several hydrogels have been used in 3D bioprinted models to provide structure to cells and to mimic ECM. Examples are gelatin [49–57], alginate [34,49–53,55,57–59], fibrinogen [49,51,55,60,61], gelatin methacryloyl (GelMA) [56,61–64], hyaluronic acid (HA) [54,63], polyethylene glycol (PEG) [65] or polyethylene glycol diacrylate (PEGDA) [54,65–67], collagen [68,69], Matrigel [70,71], and decellularized ECM [72], among others. These hydrogels possess specific characteristics, including biocompatibility, cross-linking capacity, and printability, that make them amenable to 3D printing [39,73]. They can be used alone or in combination and can be functionalized with various ECM molecules, according to the cell type and final application of the 3D bioprinted tumor model. In fact, the use of decellularized ECM in 3D bioprinted models has resulted in a higher expression of pro-angiogenic markers and ECM-remodeling proteins in cancer cells [72], thereby better recapitulating the TME than can be achieved with cells cultured in absence of ECM. Unfortunately, decellularized ECM is not always available, and some ECM-derived hydrogels, like collagen, are not printable [74]. Consequently, a combination of different hydrogels or of chemically modified hydrogels that are crosslinkable [75] is employed to generate 3D constructs that can provide cells with a suitable scaffold containing cell-adhesion sites, along with other relevant chemical and physical cues.

The TME contains cancer cells, MSCs, endothelial cells, and immune cells [3,4], but most 3D bioprinted tumor models have only been able to incorporate a limited number of different cell types. These have included combinations of cancer cells and endothelial cells [72,76] or stromal cells [34,50,57], with the third cell type being healthy epithelial cells [66,68] or immune cells [56,58]. Some research groups have also used cells that

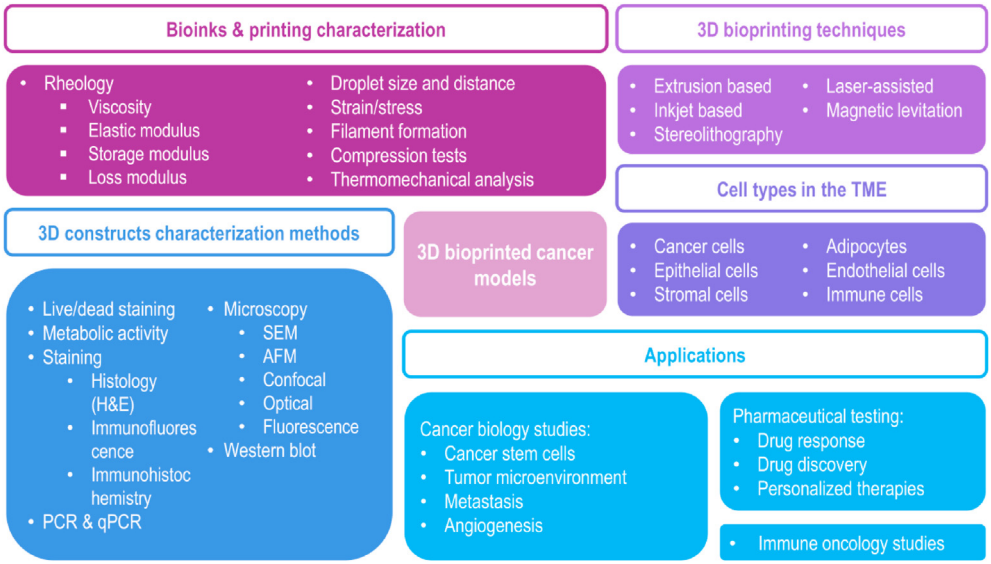

Fig. 3. 3D bioprinting of cancer models. Reported bioprinting techniques, cells present in the tumor microenvironment, characterization of bioinks and 3D constructs, and applications of printed tumor models.

are representative of other organs to fabricate metastasis models [69,77]. Patient-derived tumor organoids have even been successfully generated by immersion bioprinting, and the resulting organoids maintain their tumor heterogeneity and display similar drug responses to those seen in their tumors of origin [33].

So far, the inclusion of growth factors in bioprinted 3D tumor models has been limited to the use of EGF, which promotes cancer growth and contributes to aggressive behavior [58,64] or to the use of VEGF, which stimulates angiogenesis and regulates vascular permeability [61]. The gene expression of these and other growth factors has been measured and will be discussed further in Section 3.5.5.

Recognizing the importance of vasculature, several research groups have recently started to include microchannels or endothelial cells that can vascularize, such as human umbilical vein endothelial cells (HUVEC) [34,61,70,72,76,78,79] or microvascular endothelial cells (MVEC) [61, 76], into their 3D bioprinted models. Previous tissue engineering research has introduced several platforms for the bioprinting of artificial blood vessels and vascular grafts using cellular or acellular materials and procedures [80]. Three main methodologies have been widely reported specifically for 3D bioprinting: (a) fabrication of hydrogel matrices with integrated channels [81], (b) patterning of cells into linear structures for self-assembly of vascular networks [82], and (c) fabrication of free-standing tubular structures [83]. The objective of adding these structures is to generate relevantly sized constructs that resemble *in vivo* vascularized tumors.

3. 3D bioprinted tumor models

The use of 3D bioprinting for tumor modeling allows the generation of structures with greater complexity than can be obtained with 2D culture or scaffold-free 3D culture strategies. As shown in Fig. 4, 3D bioprinted tumors have been developed into a wide variety of structures ranging from fibers (Fig. 4A) [50,84], microbeads (Fig. 4D) [52], discs (Fig. 4E) [63], grids (Fig. 4F) [69], or multilayered grids (Fig. 4G) [53, 85], to sandwich structures [86], mini organs (Fig. 4H) [56] and customized shapes (Fig. 4I) [74]. Moreover, 3D bioprinting has been used to enhance microfluidic devices (Fig. 4J-LK) [54,61] to enable modeling of cell migration and metastasis [62,65], endothelial barrier function [76], and vascularization [49]. Table 1 summarizes recently reported 3D bioprinted models.

Even with a fully recapitulated structure, a model still relies on the complexity of the cell types and their arrangement within the construct for authentic representation of a human tumor. Success in recapitulating a particular tumor niche cannot be achieved without an adequate engineering of bioinks (i.e, the appropriate combination of materials, cells, and chemical or physical cues within the ink formulations). In the following sections, we will discuss the characterization of inks and bioinks and the increasing complexity of the tumor models that can be produced according to the number of cell types used. We will start with models based on single cell types, followed by models derived by co-culture of two or more cell types, and, finally, vascularized models.

3.1. Characterization of bioinks and bioprinting techniques

Before performing the bioprinting process, the bioink or bioinks to be used in the fabrication of the tumor model must be characterized. With the right combination and concentration of hydrogels, the bioink mixture can attain the correct viscosity and elasticity to achieve printability and generate the desired microenvironment. This allows the generation of a matrix with suitable stiffness for cell adhesion and growth.

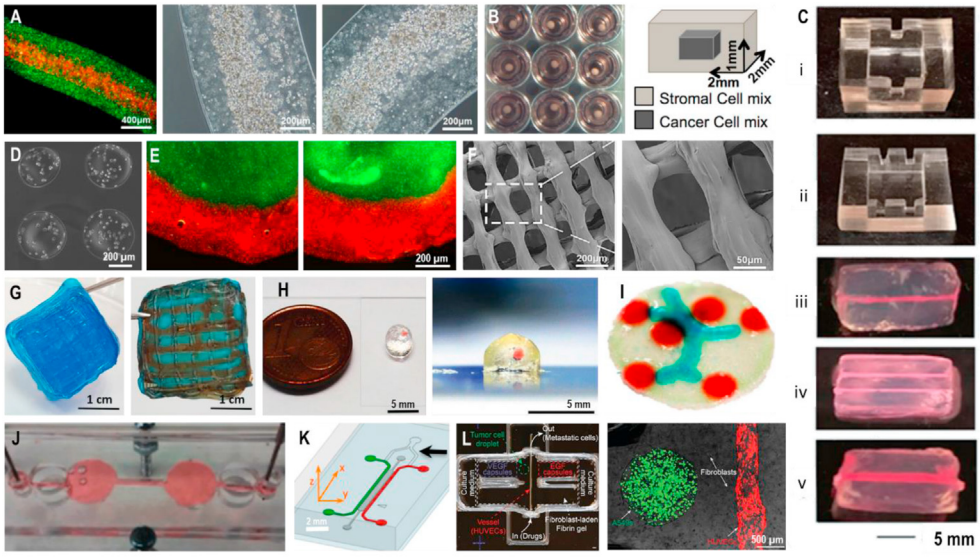

Fig. 4. Structures used for 3D bioprinted tumors. (A) Glioma shell-core hydrogel microfiber. Adapted from Ref. [84]. (B) Millimeter-scale cancer tissue bioprinted in transwell culture plates. Adapted from Ref. [34]. (C) Customized molds and gelatin methacryloyl (GelMA) constructs designed for a lymphangiogenesis model of breast cancer. Adapted from Ref. [89]. (D) Human breast cancer microbeads. Adapted from Ref. [52]. (E) Breast cancer disks with 21 PT (epidermal growth factor receptor [HER] 2+) breast tumor cells in the middle and adipose-derived mesenchymal stem cells (ADMSC) surrounding them. Adapted from Ref. [63]. (F) Scanning electron microscopy (SEM) image of glioma cell-laden hydrogel grids. Adapted from Ref. [55]. (G) A bioprinted perfusable construct comprising glioma stem cells and mesenchymal stem cells (MSCs). Adapted from Ref. [50]. (H) Bioprinted mini-tissue with a glioblastoma area highlighted in red. Adapted from Ref. [56]. (I) A customized bioprinted cancer model. Adapted from Ref. [74]. (J) A colon cancer metastasis-on-a-chip device. Adapted from Ref. [54]. (K) Microfluidic tumor-vascular interface device with endothelial channel (green), tumor channel (red), and 3D extracellular matrix (dark gray). Adapted from Ref. [76]. (L) 3D bioprinted metastatic model for guided tumor cell migration. Adapted from Ref. [61]. (For interpretation of the references to color in this figure legend, the reader is referred to the Web version of this article.)

Table 1
Current cancer models generated by 3D bioprinting.

Cell lines	Hydrogel	Size	3D bioprinting technique	Vascularized	Characterization	Application	Bioprinter	Ref.
Single cell models								
Glioma stem cells (GSCs)	Modified porous: Gelatin Alginate Fibrinogen	–	Extrusion	No	Nestin expression for stem cells Glial fibrillary acidic protein and β-tubulin III expression for differentiation IHC of VEGF	Vascularization Tumor biology Drug resistance and susceptibility	3D multi-nozzle bioprinter (Tissform III)	[49]
Glioma stem cells (GSCs)	Gelatin Alginate Fibrinogen	15 × 15 mm, 1 mm thickness	Extrusion	No	Cell viability TEM Stemness properties Expression of tumor angiogenesis-related genes Vascularization potential	Tumor biology Drug resistance Vascularization	3D multi-nozzle bioprinter (Tissform III)	[55]
Glioblastoma cells (U87MG)	Fibrin Alginate	–	Extrusion	No	Cell viability Cancer stem cells and metastatic invasiveness markers	Drug screening	Aspect Biosystems RX1 bioprinter	[60]
Glioma stem cells (GSC23)	Gelatin Sodium alginate	Round grid scaffolds 15 mm diameter, 1 mm thickness	Extrusion	No	Cell viability Morphology Proliferation qPCR of angiogenesis and stemness markers Histology Flow cytometry	Tumor biology Vascularization	3D multi-nozzle bioprinter (Tissform III)	[59]
Breast cancer cells (MCF7)	PEG Gelatin	480–530 μm radius	Micro casting	No	Spheroid formation Live/dead staining Cell viability	Tumor spheroid formation	Custom-made pressure assisted value-based bioprinting system	[96]
Breast cancer cells (MDA-MB-231)	Alginate Gelatin (sacrificial)	Microbead diameters of ~100 μm and ~175 μm	Laser-direct write (LDW)	No	Cell viability (life dead staining kit) Optical coherence tomography Cell staining Confocal microscopy	Tumor spheroid formation	LDW system (Teosys LLC)	[52]
Breast cancer cells (MCF-7) or (MDA-MB) or (MCF-12A)	Decellularized ECM from rat mammary tissue	–	Extrusion	No	Histology Immunofluorescent staining RT-PCR	Tumor biology	Custom made bioprinter	[93]
Breast cancer cells (MCF7)	–	–	Thermal inkjet	No	Viability Apoptosis Phosphorylation RNA sequence analysis	Tumor biology	HP thermal inkjet printer	[97]
Breast cancer cells (MDA-MB-231)	Alginate Gelatin	10 × 10 × 1.5 mm3	Extrusion	No	Microindentation Confocal microscopy	Tumor biology	BioScaffolder 3.1 GeSiM, Germany	[98]
Cervical cancer cells (HeLa)	Gelatin Alginate Fibrinogen	10 × 10 × 2 mm	Extrusion	No	Cell proliferation MMP expression Chemoresistance	Tumor biology Drug resistance	Custom made bioprinter	[89]
Cervical cancer cells (HeLa)	Gelatin Alginate Matrigel	10 × 10 × 2 mm3 (six layers)	Extrusion	No	Live/dead staining Proliferation with cell counting kit Contrast phase microscopy Immunofluorescent staining Drug testing qRT-PCR Immunoblotting	Tumor biology Drug screening	Custom-made bioprinter	[85]
Hepatoma cells (HepG2)	Alginate Fibrinogen Gelatin	10 × 10 × 5 mm	Extrusion	No	Scanning electron microscopy, acridine orange/propidium iodide staining Cell counting kit Alpha-fetoprotein assay	Drug screening	3D controlled assembling technique	[51]
Liver cancer cells (HepG2)	Collagen Hyaluronic acid	20 μL	Extrusion	No	Viability and proliferation Drug testing	Drug screening	Cellink Incredible bioprinter	[33]
Colon cancer cells (Caco2)	Collagen Hyaluronic acid	20 μL	Extrusion	No	Viability and proliferation Drug testing	Drug screening	Cellink Incredible bioprinter	[33]
Lung cancer cells (A549 or 95-D)	Gelatin Sodium alginate		Extrusion	No	Live/dead staining Morphological	Tumor biology Invasion	Multi-nozzle bioprinter(Livprint	[53]

(*continued on next page*)

Table 1 (*continued*)

Cell lines	Hydrogel	Size	3D bioprinting technique	Vascularized	Characterization	Application	Bioprinter	Ref.
		12 mm × 12 mm (eight layers)			characterization with SEM Cell invasion with qPCR of invasion genes Cell migration with scratch test Invasion capability with transwell assay		Norm, Medprin, China)	
Rat acinar cell line (AR42J-B-13)	GelMA	10 × 10 spot array, 750 μm spacing	Laser-assisted	No	Metabolic activity Spheroid size Histology	Tumor biology	Custom-made bioprinter	[99]
Multiple cell models Breast carcinoma cells (MDA-231) Endothelial cells (MVEC & HUVEC) Murine macrophages (RAW264.7)	ECM hydrogel	–	Extrusion	Yes	Diffusive permeability of endothelial monolayer Cell imaging to track tumor cell centroids	Vascularization Endothelial barrier function	Manual	[76]
Normal breast epithelial cells (HMLE) Twist-transformed cells (HMLET)	PEGDA	3 × 3 × 1 mm	Photolithography	No	SEM Confocal microscopy (Z-stacks for 10–15 h at 20 min intervals)	Tumor biology Migration	Custom-made bioprinting system	[66]
Breast cancer cells Adipocytes Mammary fibroblasts Endothelial cells	None	–	Extrusion	Yes	Stability and viability for model Cytotoxic effects of chemotherapeutic drugs assessed biochemically and histologically	Vascularization Drug resistance	Organovo's NovoGen BioprintingTM Platform	[78]
Breast cancer cells (MDA-MB-321) Human bone marrow derived MSCs	PLA Nanocrystalline hydroxyapatite	–	Extrusion	No	SEM Adhesion Proliferation	Metastasis	Fused deposition modeling (FDM) based 3D bioprinting system	[77]
Breast cancer cells (MDA-MB-231) Murine macrophages (RAW264.7)	Alginate	–	Extrusion	No	SEM Cell viability (trypan blue) Cell migration DAPI staining	Tumor biology Migration Drug screening	Custom-made bioprinter	[58]
Breast cancer cells (MDA-MB-231 or MCF-7) Bone marrow MSCs	Nano-ink: Hydroxyapatite nanoparticles PEG or PEG-DA	Three 400 μm thick layers	Stereolithography	No	SEM Spheroid formation Drug resistance Metastasis	Tumor biology Drug sensitivity Metastasis	Printrbot® rapid prototyping platform	[65]
Breast cancer cells (MDA-MB-231) Osteoblasts (CRL-11372) or primary bone marrow MSCs	GelMA Nanocrystalline hydroxyapatite	–	Stereolithography	No	Proliferation Gene expression Alkaline phosphatase activity	Tumor biology Metastasis	Tabletop stereolithography 3D bioprinter	[62]
Breast cancer cells (MDA-MB-231 or MCF7) Normal mammary epithelial cells (MCF10A)	GelMa	100 μm depth, 500 μm diameter	Two-step photolithography	No	Live/dead Proliferation Immunofluorescence Cell tracking (migration)	Tumor biology Invasion	Custom-made bioprinting system	[64]
Breast cancer cells (MDA-MB-231 or SUM159) Fibroblasts (293T or Hs578bst)	–	–	Magnetic bioprinting	No	Live/dead Drug toxicity IHC Immunostaining	Tumor spheroid formation Drug resistance	Nanoshuttle n3D Biosciences	[111]
Breast cancer cells (MDA-MB-231) Fibroblasts (IMR-90)	Alginate Gelatin	Propeller model with internal circle of 7.7 mm diameter and external sectors radius of 8.65 mm. Four layers of 150 μm thickness	Multi-nozzle extrusion	No	Spheroid formation and size (confocal microscopy) Cell viability (MTS)	Tumor biology Migration	3D bioprinter BioScaffolder 3.1	[57]

(*continued on next page*)

Table 1 (*continued*)

Cell lines	Hydrogel	Size	3D bioprinting technique	Vascularized	Characterization	Application	Bioprinter	Ref.
Breast cancer cells (21 PT) Primary human adipose derived MSCs (ADMSC)	Methacrylated hyaluronic acid GelMA	21 PT laden regions ~6 mm in diameter, ~1.2 mm in thickness, ADMSC regions ~400 μm in thickness	Extrusion	No	Drug resistance (MTT assay) Immunofluorescent staining Cytotoxicity, atomic force microscopy (AFM) nanoindentation, LOX activity, and qPCR analysis	Drug resistance	3D Bioplotter, EnvisionTEC	[63]
Breast cancer cells (MCF-7 or MDA-MB-468) Normal mammary epithelial cells	Rat tail collagen	Volumes >0.001 mm3	Extrusion	No	Invasiveness Immunostaining	Tumor biology	Fully customized Felix 3.0	[68]
Breast cancer cells (MCF-7, MDA-MB-231, MCF10A-NeuN) Endothelial cells (HUVEC)	Matrigel	–	Extrusion	Yes	Viability Architecture Function Drug resistance	Drug resistance	Custom-made dual nozzle bio-deposition system	[70]
Breast cancer cells (MCF-7) Primary human mammary fibroblasts (HMFs) Endothelial cells (HUVEC)	Sodium alginate	2 mm × 2 mm x 1 mm	Extrusion	Yes	Histology Immunostaining Light-sheet microscopy Leptin secretion qPCR Drug resistance	Tumor biology Drug resistance	Organovo's Novogen MMX Bioprinter Platform	[34]
Breast cancer cells (MBA-MD-231) Human dermal lymphatic microvascular endothelial cells (LECs)	GelMA Agarose	10 × 8 × 4 mm3	Extrusion	Yes	Immunofluorescent staining Migration Metastasis	Tumor biology	Custom-made bioprinter	[105]
Breast cancer cells (MCF7) Adipose-derived stromal cells (ADSCs)	Alginate Gelatin	–	Extrusion	No	SEM Viability Metabolic activity Adipogenic potential	Tumor biology	Tissue Scribe Gen. 3 printer, 3D Cultures	[112]
Glioma stem cells (GSC23) Human mesenchymal stem cells (MSCs)	Alginate Gelatin	Fibers of ~243 μm and ~871 μm	Coaxial extrusion	No	Live/dead assay Proliferation Histological and immunohistological analyses Masson staining qRT-PCR	Tumor biology	Custom-made computer-controlled coaxial extruding bioprinting system	[50]
Shell-glioma stem cells (GSC23) Core-glioma cell line (U118)	Sodium alginate	867.53 μm diameter fibers	Coaxial extrusion	No	Tumor invasion and drug resistance markers expression qPCR Western blot Cell-cell interaction Cell viability (live/dead) Cell proliferation Alamar Blue SEM Drug resistance (Alamar Blue) DNA methylation level	Tumor biology Drug resistance	Custom-made coaxial extrusion bioprinting device	[84]
iPSC-derived human neural progenitor cells Glioma cells (U118)	–	–	Extrusion	No	3D confocal microscopy	Invasion	Regenova 3D bioprinter, Cyfuse Biomedial K. K.	[107]
Glioblastoma cells (GL261) Macrophages (RAW264.7)	GelMA Gelatin	5 × 4 × 6 mm	Extrusion	No	Cell viability qPCR immunostaining invasion & proliferation	Tumor biology Drug screening	Custom-made bioprinter	[56]
Glioblastoma (biopsies) Endothelial cells (HUVEC)	Decellularized ECM from brain tissue	–	Extrusion	Yes	Invasion Oxygen concentration distribution mRNA expression with qPCR Histology and DAPI staining	Tumor biology Drug screening	In-house 3D-printing system	[72]

(*continued on next page*)

Table 1 (*continued*)

Cell lines	Hydrogel	Size	3D bioprinting technique	Vascularized	Characterization	Application	Bioprinter	Ref.
					Immunostaining Pharmacological tests			
Glioblastoma cells (U87MG) Monocyte/ macrophages (MM6) Glioblastoma stem cells (GSCs) Glioma associated stromal cells (GASCs) Microglia.	Alginate modified with RGDS cell adhesion peptides Hyaluronic acid Collagen 1.	–	Multi-nozzle extrusion	No	Cell proliferation and viability Protein kinase activity Drug sensitivity	Tumor biology Drug sensitivity	Modified open-source Fab@Home dual syringe printer	[75]
Glioblastoma cells (U87 MG) Endothelial cells (HUVEC) Lung fibroblasts (LFs)	Gelatin Alginate Fibrinogen	10 × 10 × 0.6 mm3	Extrusion	Yes	Immunostaining RT-PCR Drug response	Drug screening	INVIVO bioprinter, ROKIT healthcare	[90]
Human bone marrow-derived epithelial-neuroblastoma cells (SH-SY5Y) Umbilical cord-derived MSCs (UC-MSCs) Endothelial cells (HUVEC)	Agarose Collagen type I	7 cm2	Extrusion	Yes	Histology Immunostaining	Tumor biology	Custom-made multi nozzle bioprinter	[74]
Ovarian cancer cells (OVCAR5) Normal human fibroblasts (MRC5)	Matrigel	–	Inkjet	No	Photodynamic therapy response Drug response Live/dead fluorescence	Tumor biology Drug screening	Precision Linear Stage, Newmark systems, NLS4	[95]
Ovarian cancer cells (OVCAR5) Normal human fibroblasts (MRC-5)	Matrigel	–	Inkjet	No	Size of droplet Live/dead Dark-field microscopy (acini growth) Two-photon imaging	Tumor spheroid formation	Custom-made bioprinting system	[71]
Cervical cancer cells (HeLa) Mouse embryo cells (10T1/2)	PEGDA	Honeycomb designs with 25, 45, and 120-μm-wide channels	Stereolithography	No	Migration Cell morphology Time lapse microscopy	Migration	DMD-PP Printing System	[67]
Human fibrosarcoma cells (HT1080) Endothelial cells (MVEC)	ECM hydrogel	–	Extrusion	Yes	Tumor-Endothelial Intravasation	Vascularization Endothelial barrier function	Manual	[76]
Colon cancer cells (HCT-116 or SW480) Intestine epithelial cells (INT-407) Liver cells (HepG2)	Thiolated hyaluronic acid Thiolated gelatin Polyethylene glycol diacrylate (PEGDA)-based hydrogel	–	Extrusion	No	Expression of normal epithelial markers (ZO-1 proteins, β-catenin and vinculin), mesenchymal and proliferative markers	Tumor biology Metastasis Drug screening	Manual	[54]
Oral squamous cell carcinoma Oral keratinocytes Oral fibroblasts Alveolar human osteoblasts	Collagen Agarose B-tricalcium phosphate	Disc of 10 × 2 mm	–	No	IHC of cytokeratin 13 & 14 Histology Immunostaining SEM qRT-PCR	Tumor biology Invasion	EnvisionTEC 3D bioprinter	[69]
Pulmonary cancer cells (A549) Stromal cells Endothelial cells (HUVEC)	GelMA Fibrinogen	–	Inkjet	Yes	Programmable release capsules with growth factors Proliferation and migration Metastasis Fluorescent staining Anticancer drug screening	Tumor biology Invasion Metastasis Vascularization Drug screening	Custom-made bioprinter	[61]
Human hepatocellular carcinoma (SMMC-7721)	Hydroxymethyl chitin	25 × 25 mm area and 6 layers height	Extrusion	Yes	Migration, proliferation Protein expression level Tumor migration & proliferation	Drug screening	Custom extrusion-based 3D cell printer	[79]

(*continued on next page*)

Table 1 (*continued*)

Cell lines	Hydrogel	Size	3D bioprinting technique	Vascularized	Characterization	Application	Bioprinter	Ref.
Endothelial cells (PUMC-HUVEC-T1) Peripheral blood mononuclear cells					Tumor invasion/cluster size Protein secretion Immune effects Protein secretion Immunofluorescent staining			
Patient-derived pancreatic cancer cells Primary pancreatic stellate cells Endothelial cells (HUVEC)	Sodium alginate	2 mm × 2 mm x 1 mm	Extrusion	Yes	qPCR Drug resistance	Tumor biology Drug resistance	Organovo's Novogen MMX Bioprinter Platform	[34]

3.1.1. *Extrusion bioprinting*

Bioink properties are key determinants of the performance of a bioprinting procedure. Therefore, characterization of the bioink properties is vital. For any kind of bioprinting, evaluation of how cell densities and temperature may influence rheology and consequently printability is an important step. For extrusion bioprinting, the bioinks must be able to flow through a nozzle or a needle to form a filament, while still retaining the ability to assume their 3D shape after deposition and to support the weight of material deposited on top without collapsing [87]. No standardized method exists for characterizing a material's printability; however, viscosity is the most important property that determines printability. Viscosity can be characterized by rheological analysis, in which variables such as shear-thinning behavior (decrease of viscosity under shear strain), yield stress, storage and loss modulus are measured. Recently, methods based on the use of printability indicators, such as the parameter optimization index (POI), have been introduced to standardize extrusion processes [88]. The following are some illustrative examples of the rheological characterization of bioinks used to bioprint TMEs.

Rheological properties were assessed in a bioink composed of alginate, gelatin, fibrinogen, and HeLa cells (human cervical cancer cells) to determine the extrusion parameters. The assessment was performed using a rotational rheometer with a shear rate of 100 s^{-1} and a temperature change from 30 °C to 8 °C. Results showed an increase in viscosity between 20 °C and 10 °C. In addition, a decrease in cell survival rate was observed above 25 °C. Therefore, the chosen parameters were 10 °C for the chamber temperature and 25 °C for the nozzle temperature for printing 3D HeLa/hydrogel constructs. Decreasing the chamber or nozzle temperature caused a higher hydrogel viscosity and less cell viability after 3D bioprinting [89].

In a similar study, a mixture of 3% alginate and 7% gelatin was evaluated for multi-cartridge extrusion bioprinting. The rheological properties were assessed using a temperature and time sweep to analyze thixotropy (time-dependent shear-thinning behavior) and flow curves. The temperature sweep, which was run with a gradient from 25 °C to 37 °C, resulted in a decrease in both storage (G', 468.5 ± 34.2 Pa to 3.2 ± 0.2 Pa) and loss (G'', 140.7 ± 9.3 Pa to 11.8 ± 0.6 Pa) moduli. This corresponded to a secondary structure denaturation of the gelatin fibers, which then displayed a liquid-like behavior. The transition temperature from solid to liquid for the hydrogels was 30.6 °C when both the storage and loss moduli were 51.7 ± 9.7 Pa. The gelation time sweep was measured when the hydrogel was removed from a 32 °C water bath and placed on a 25 °C rheometer platform at a 1HZ frequency. The sol-gel transition occurred after ~30 min, and the viscosity then rose until optimal printing characteristics were achieved between 50 and 90 min. Optimal printing conditions were determined as 200 kPa pressure and a 5 mm s^{-1} print speed. Thixotropy tests, made to simulate the mixing and extrusion processes by applying different shear rates, showed that gelation kinetics were not affected by low shear (15 s^{-1}), despite a minor viscosity decrease. Even after being subjected to a high shear rate, the broken gel reassumed its gel form in 4 min, confirming the stability of the 3D construct before crosslinking. The flow curve tests showed that the ink displayed a decreasing viscosity with an increasing shear rate, thereby confirming the shear thinning property of this hydrogel mixture [57].

The interplay between the bioink properties and the extrusion conditions influences the characteristics of the printed structures. For example, when a hydrogel mixture of alginate/gelatin (A/G) was used as the shell of a core-shell fiber structure fabricated by coaxial extrusion, the resulting inner and outer diameters of the A/G shell were ~243 and ~871 μm when the extrusion rates were 30 mL h^{-1} for the A/G and 3 mL h^{-1} for the cell suspension. Conversely, the inner diameter of the A/G shell increased to ~527 μm while the outer diameter remained the same (~887 μm) when the extrusion rate of the cell suspension was set at 10 mL h^{-1}. Therefore, adjusting the extrusion rates can change the shell's inner diameter without affecting the outer diameter [50]. Consequently, when hydrogels are combined, assessment of the new rheological properties displayed by the blend becomes important. The rheological evaluation of a gelatin/alginate/fibrinogen mixture that used a frequency sweep from 0.1 Hz to 100 Hz at 1% strain at standard room temperature resulted in storage and loss moduli of 0.7–9 and 0.06–1.7 kPa, respectively [90].

A previous study compared non-bioprintable (0.3% collagen) and bioprintable (0.5% agarose-0.2% collagen) bioinks by performing oscillatory tests in a rotational rheometer. The authors used a five-step oscillatory sequence and recorded the storage and loss moduli. An increase in the frequency and strain of the storage and loss moduli of the non-bioprintable bioink was noted, whereas the bioprintable bioink showed relatively constant parameters. Furthermore, after the application of a frequency sweep from 0.5 to 50 Hz to both bioinks, the initial values for the storage and loss moduli of the agarose-collagen bioink were restored, whereas the collagen bioink retained the ten-fold increase in those parameters [74]. The shear stress present during the bioprinting process predicted a possible gelation of the collagen ink inside the printer head, which could lead to clogging. The authors therefore chose to use the agarose-collagen bioink for subsequent bioprinting experiments.

Thermomechanical analysis is also an important consideration when characterizing bioinks. The objective of a thermomechanical analysis is to assess how the bioink behavior is influenced by mechanical and thermal stimuli present during the bioprinting process. A bioink composed of alginate modified with RGDS cell adhesion peptides (RGDS-alginate), hyaluronic acid, collagen-1, and glioblastoma cells was subjected to compression tests in a 2980 dynamic mechanical analyzer (DMA) with a ramp force from 0.1 to 1 N for 10 min, at room temperature. Calculation of the elastic modulus with the slope of the stress-strain curve demonstrated that an increase in the $CaCl_2$ concentration for crosslinking from 10 to 50 mM gave a higher stiffness values of 11.9 and 25.7 kPA, respectively, in 2% alginate hydrogels [75].

Matrigel has also largely been used as a hydrogel to support the

growth of cancer cell lines in 3D models. Recent research has shown that after rheological characterization, the printing parameters for Matrigel were 22–24 °C, 3–7 kPa pressure, and crosslinking at 37 °C for 30 min. After being bioprinted in Matrigel, melanoma cells were able to spread, proliferate, and form networks throughout the construct [91].

Other hydrogels, such as Matrigel mixed with hydroxypropyl chitin (HPCH), can be bioprinted by extrusion. This ink was characterized in a rheometer using an oscillation test with low frequency (1 Hz) and amplitude gamma-band (0.1% as constraints) at various temperatures (4 °C–37 °C). The storage modulus increased with a rising temperature, and when it reached 18 °C, it exceeded the loss modulus, thereby reaching the gelation temperature. The hydrogel was therefore deemed suitable for extrusion at 18 °C and for crosslinking at 37 °C [79].

Another example of an ink matrix is hyaluronic acid (HA). A composite hydrogel precursor of acrylated-HA (HA-AC) and HA modified with sulfhydryl groups (HA-SH) was synthesized for the generation of prostate cancer constructs, and the rheological properties of this hydrogel were evaluated with a controlled stress rheometer. The researchers determined the linear viscoelastic region by a strain sweep from 0.1 to 1000% using an angular frequency of 6 rad/s. Within this linear range, they also performed a frequency sweep experiment at 1% strain from 0.1 to 100 rad/s and a time sweep experiment for 6 h at a frequency of 6 rad/s. They showed that the composite hydrogel had an average storage and loss moduli of 234 ± 30 and 3 ± 2 Pa. Gelation started at 17 min after the mixing of the HA-AC and HA-SH but finished after 6 h. The hydrogels were insensitive to the frequency change from 0.1 to 10 Hz, confirming the elastic nature of the HA-AC/HA-SH networks [92].

One variation of extrusion is immersion bioprinting. This approach first requires characterization of a hydrogel that will work as an immersion bath. Recent research has evaluated three gelatin concentrations (5, 10, and 20 mg/mL) for use as immersion baths with bioinks based on a collagen-hyaluronic acid mixture and a HyStem hydrogel. The pertinent rheological tests were conducted using a strain sweep from 1% to 1000% shear strain, and the storage and loss moduli of each material were measured. The researchers determined that the optimal gelatin concentration of the immersion bath was 10 mg/mL and that the best bioink was collagen-hyaluronic acid [33].

Decellularized tissues derived from rat and human breast (rtMECM & huMECM) have also been characterized for use as inks for immersion bioprinting of mammary tumoroids and organoids. To achieve spontaneous gelation, the hydrogels were prepared in concentrations ranging from 10.4 to 0.7 mg/mL, with successful gelation down to 1.3 mg/mL. Thus, the standard concentration chosen was 2.6 mg/mL. The rheological properties of these ECM-derived hydrogels were then assessed by measuring the Young's modulus using an unconfined compression test that induced only lateral deformation of the hydrogels. The force required to compress the gels was recorded to deduce the stress vs. strain ratio. The resulting yield strengths were 39 ± 9 and 42 ± 6 kPa for the rtMECM and huMECM, respectively. These characteristics allowed the growth and spread of MCF-12A, MCF-7, and MDA-MB-468 cells [93].

These reports confirm the need for standardized characterization methods for extrusion bioprinting, but rheology and thermomechanical analyses are a good start in fulfilling this requirement.

3.1.2. Laser-assisted bioprinting

Laser-assisted bioprinting is influenced by the laser parameters, the air gap between the donor and collection layers, and the bioink viscosity. Thus, the effectiveness of the bioinks for this bioprinting technique relies entirely in the viscosity, which is sometimes modified by cell density [94]. Therefore, the bioink characterization goes hand in hand with the technique characterization.

Characterization of bioinks for laser direct-write (LDW) differs from that performed for extrusion because the technique uses a pulsed laser to deposit the material. That, coupled with the absence of a nozzle, gives more precise control of the spatial patterning and the size of the cell microbeads. An alginate ink was characterized to determine if cell seeding densities of the print ribbon could be used to control the size and cell density of the alginate microbeads. In this study, the authors created two arrays at small (100 μm) and large (175 μm) beam diameters for five ribbon cell densities ranging from 1.0×10^6 to 10×10^6 cells mL^{-1}. The beam size was measured by pulsing the laser on an ink-covered glass slide, and it was then recorded using an Opher energy meter displaying mean energies of 3.05 ± 0.66 μJ for the small beam and 5.01 ± 1.21 μJ for the large beam. The printed microbead arrays were analyzed for size and cell number. Alginate beads printed with a small beam had a 200 μm diameter and contained 3–21 cells, whereas beads printed with a large beam had a 400 μm diameter and contained 15–157 cells [52]. These results demonstrate that the size of the microbeads printed by LDW can be controlled by the beam diameter and that the cell number is highly variable but largely depends on the initial cell loading.

From this, we can elucidate that fabrication of a predesigned 3D structure requires a bioink that can be quickly crosslinked, but bioinks with various surface tensions and viscosities can be employed.

3.1.3. Inkjet bioprinting

Inkjet bioprinting, unlike laser-assisted bioprinting, must use bioinks with low viscosities and cell densities. An important parameter is the bioink surface tension since it determines if the printing process will result in the formation of droplets or a jet. Importantly, surface tension is related to the cell concentration; when the cell concentration increases, the surface tension decreases. The gelation of the bioink must also happen *in situ* after the material is deposited to avoid blockages inside the nozzle [94].

One of the key aspects that has been evaluated for this bioprinting technique is the droplet size. For example, one group of researchers ejected Matrigel-encapsulated ovarian cancer cells into a Petri dish filled with nitrogen to freeze the droplets for analysis by microscopy. Two parameters were measured: droplet size and cells per droplet. The valve opening time and the gas pressure were maintained constant (60 μs at 34.5 kPa) because they determine the ejection speed and droplet size. The droplet diameters were obtained by fitting circles around each droplet, and a constant droplet diameter of 900 μm was observed [95]. Another study by the same research group involved analysis of droplet placement and inter-droplet distance using the same bioink to assess the spatial patterning precision, as well as the droplet size. The droplet deposition varied between 4.9 μm and 18 μm in the distal and proximal directions, respectively. The difference between the programmed distance and the printed distance was less than 3.5%, and the droplet size obtained was ~510 μm [71].

Both studies demonstrate that the number of cells per droplet used for inkjet bioprinting depends on the initial cell loading and the droplet size, similar to laser-assisted bioprinting. By contrast, the droplet size depends on the valve opening time and pressure, as well as the ejection distance.

3.2. Simple models: single cell type

The high global incidence of breast cancer has demanded the use of rather simple single-cell models to represent it. The most reported method used to model breast cancer with 3D bioprinting is spheroid fabrication. For instance, spheroids have been produced by generating cell-laden beads through LDW, a controlled production process that can create tumor spheroids of a regular size and shape [52]. Breast cancer spheroids can also be generated using sacrificial gelatin arrays in PEG concave wells, which allows uniform *in situ* cell seeding and spheroid formation with MCF-7 cells [96]. Some breast cancer models have been studied to assess the effect of the bioprinting process in phosphorylation and gene expression in cell pathways associated with biologically aggressive oncogenic properties [97]. Other models have focused on the physical properties of the embedding hydrogel to ensure that it provides a suitable environment that replicates both the mechanical and biochemical characteristics of the tumor stroma [98].

Some of the most widely reported 3D bioprinted single-cell tumor

models are brain tumor models. One 3D bioprinted glioma stem cell model was generated by combining gelatin, alginate, fibrinogen, and glioma stem cells in a multilayered grid construct [49,55]. Despite the simplicity of this model, it has proved useful for studying cancer biology, tumor recurrence, and drug resistance. A fibrin-based glioblastoma (GBM) model printed in a ring structure showed high viability even after 12 days of culture [60]. A model fabricated with the GSC23 glioma stem cell line in sodium alginate and gelatin was printed in a round grid shape. The printed cells proliferated better than cells in suspension culture and had a higher endotheliogenic potential [59].

Multilayered grid structures have also been fabricated by extrusion 3D bioprinting to represent liver, cervical, and lung tumor models through extrusion 3D bioprinting. A liver model was generated by combining alginate, gelatin and fibrinogen with HepG2 cells [51]. Similarly, cervical tumor models were generated using HeLa cells, gelatin, alginate, and either Matrigel or fibrinogen [85,89]. For lung cancer, the A549 or 95-D lung cancer cell lines were encapsulated in hydrogels composed of gelatin and sodium alginate, and the 3D constructs remained structurally intact for up to 28 days of culture [53]. Simpler structures, such as dot arrays, have recently been used to bioprint acinar cell spheroids to assess their trans-differentiation into ductal cells for the study of pancreatic ductal adenocarcinoma [99]. The latest research has managed to fabricate tumor organoids (hepatic and colon cancer cell lines, as well as patient-derived glioblastoma and sarcoma) by immersion bioprinting in collagen/hyaluronic acid hydrogels and has used these for high-throughput drug screening [33].

Bioprinting may enable easier, more reproducible, and faster fabrication of spheroids than conventional methods (i.e., drop-hanging, high cell density seeding in ultra-low adherence surfaces, and agitation methods). Bioprinting may also greatly enable faster [100] medium-to-high throughput fabrication [100,101] of homogeneous and monodisperse populations of cancer spheroids; where uniformity in size and shape [52] is a key aim for drug screening applications. As an additional note, a distinction should be made between using bioprinting to fabricate spheroids and using hydrogels containing spheroids to build more sophisticated cancer models. Bioprinting using inks loaded with spheroids is especially useful for cancer research because it allows the emulation of a real tumor by seeding cancer spheroids into a stromal cell-laden matrix hydrogel [34,61,78,102].

Single-cell models have been useful as proof-of-concept models that confirm the possibility of bioprinting cancer cells, but their application is sometimes limited due to the lack of other relevant cell types in the model. For this reason, the addition of stromal or immune cells has become popular as a way to improve tumor models and to increase their complexity and broaden their applications.

3.3. Co-culture of cancer cells and other cell types

Co-culture of cancer and other cell types greatly improves the recapitulation of the tumor microenvironment. The inclusion of multiple cell types is evidently a must in studies related to migration/metastasis and to the interactions of cancer cells with auxiliary cells [103], and multicellular models can also be used to study cancer metastasis. The 3D bioprinting of multiple cell types can be combined with microfluidics to generate “metastasis-on-a-chip” models that allow evaluation of tumor metastasis by migration measurements and biomarker expression [54]. These multicellular models can be also used to study the tumor stromal interaction by co-culturing cancer cells together with MSCs [50,71]. On the other hand, the co-culture of cancer cells with immune cells allows the assessment of the antitumor potential of immunomodulatory antibodies [104]. As sections 3.3.1 through 3.3.3 show, the majority of bioprinted cancer models are breast cancer and GBM models, but other types of cancer, such as colon, ovarian, and oral cancer, have also been modeled.

3.3.1. Breast cancer models

Breast cancer models have been fabricated to study tumorigenesis and cell migration using several breast cancer cell lines (MCF-7, MDA-MB-231, and MDA-MB-468) combined with normal mammary epithelial cells (MCF-10A and MCF-12A) [64,68]. These models have also combined cancer cells (MDA-MB-231) with fibroblasts (IMR-90) to provide proof-of-concept evidence that bioprinting of these two cell types results in the formation of multicellular tumor spheroids via migration and infiltration [57]. The co-culture of breast cancer cells (MDA-MB-231) with mouse macrophages (RAW 264.7) was a different approach taken to study the paracrine loop and 3D segregation, as well as subsequent assessment of the pharmacological effect of inhibitors of migration [58]. Other models have used multiple cell types to test the migration capability in a hydrogel matrix while varying its stiffness, thereby providing insight into the potential for tumor cells to migrate within and colonize tissues of different stiffnesses [66]. Other approaches have included the co-culture of human dermal lymphatic microvascular endothelial cells (LECs) with MDA-MB-231 breast cancer cells to study metastasis through lymphatic vessels [105]. Stromal cells (adipocyte-derived MSCs) have also been co-cultured with breast cancer cells (21 PT) to assess the effects of obesity in doxorubicin resistance; this model was deemed to reproduce *in vivo* conditions and may be useful for cancer biology studies and drug screening [63].

Breast cancer can produce metastasis in bone, lungs, liver, and brain [106], with bone being one of the primary sites. This has promoted interest in creating 3D bioprinted models that recapitulate breast cancer bone metastasis. One research group used extrusion to fabricate a model with MDA-MB-231 and bone marrow–derived MSCs. Different geometries (squares and hexagons) were created using polylactic acid (PLA) functionalized with nanocrystalline hydroxyapatites (nHA). This matrix was then used to study breast cancer bone metastasis [77]. The same group then used stereolithography to generate a different bone matrix by combining GelMA and nHA to study the interaction between breast cancer cells (MDA-MB-231) and bone stromal cells (primary human bone marrow MSCs and CRL-11372 osteoblasts) [62]. The MDA-MB-231 cells proliferated better in the presence of bone stromal cells, whereas the proliferation of bone stromal cells was inhibited by the presence of breast cancer cells. Thus, this model provided a tool for research into post-metastatic breast cancer progression in bone. The same group also used this matrix but containing only osteoblasts as stromal cells and substituting GelMA for PEG for the analysis of breast-cancer-cell spheroid formation and assessment of drug sensitivity, and they concluded that this model can mimic tumor bone microenvironments [65].

Breast cancer is the most common type of cancer among women; therefore, several studies have focused on elucidating its nature. Some of the most complex bioprinted models have tried to represent breast cancer by including normal mammary epithelial cells, fibroblasts, macrophages, and adipocytes. These models have provided several resources for researching tumor genesis, cell migration/metastasis, paracrine cell communication, and drug responses, thereby facilitating the search for better approaches to attack this disease.

3.3.2. Glioblastoma models

GBM is the most common malignant primary brain tumor. Several models have been 3D bioprinted by combining glioma stem cells with MSCs, macrophages, and glioblastoma-associated stromal cells.

For the study of GBM biology, sodium alginate and fibrinogen microfibers containing GSC23 glioma stem cells and MSCs were bioprinted by coaxial extrusion to study cell-cell interactions between tumor cells and MSC-derived stromal cells [50]. The research group used a CRE-LOXP switch gene system and discovered that tumor stroma cells interacted with each other and fused, thereby expressing red fluorescent protein (RFP). The researchers concluded that these fibers are a good model for studying the tumor microenvironment *in vitro*. A similar study bioprinted sodium alginate microfibers comprised of GSC23 shell-glioma stem cells and the U118 core-glioma cell line to study cell-cell

interactions [84]. In this model, the expression of tumor invasion and drug resistance markers, such as MMP2, MMP9, VEGFR2, and O-6-methylguanine-DNA methyltransferase (MGMT), was significantly enhanced when compared to a U118 cell culture alone.

GBM cells have also been co-cultured with macrophages because of the known involvement of macrophages in the progression and invasiveness of this kind of cancer. Thus, micro-tissues were fabricated using a combination of GL261 mouse glioblastoma cells and RAW264.7 mouse macrophages in a GelMA-gelatin bioink to assess the interaction between these cell types and to test drugs that target this interaction [56]. The GBM cells were found to recruit macrophages and turn them into GBM-associated macrophages, which then induced GBM cell progression and invasiveness. Similar models were generated by combining U87MG glioblastoma cells and MM6 monocyte/macrophages, or glioblastoma stem cells (GSCs), glioma associated stromal cells (GASCs), and microglia, with alginate modified with RGD sites [75]. The 3D constructs comprising GBM cells alone or co-cultured with macrophages were then exposed to cisplatin or TMZ to determine drug sensitivity, and the constructs containing macrophages showed less drug sensitivity compared to the cancer cells alone. This model was deemed suitable for studying the tumor microenvironment and for use in preclinical drug sensitivity testing.

A different approach for generating GBM models involves scaffold-free 3D bioprinting using needle arrays to bioprint spheroids. This platform was used to create an invasion model that combined spheroids derived from mouse neural progenitor cells and U118 glioma cells [107]. Examination of these organoids by 3D laser scanning confocal microscopy in real time and in fixed samples confirmed that invasion could be followed using this technique and indicated that this was potentially a model for defining personalized treatments.

These glioblastoma bioprinted models have managed to better recapitulate the *in vivo* conditions of this type of brain tumor by including stromal cells such as MSCs, microglia, and other macrophages. Tumor stromal cells and the acellular components of the tumor niche are known to modulate the tumor's drug response and development. Therefore, these models are a valuable representation of real glioblastoma tumors and provide resources to find new therapeutic targets.

3.3.3. Other types of cancer

Ovarian cancer has not been frequently explored with 3D bioprinting, although models comprising ovarian cancer cells (OVCAR5) co-cultured with fibroblasts (MRC5) have been used to assess cell viability after bioprinting through inkjet micropatterning and acinar formation [71]. This model was also used to assess mechanism-based combination treatment regimens with photodynamic therapy (PDT) and showed that PDT provides a synergistic enhancement of the efficacy of carboplatin depending on the treatment application sequence [95].

Colon cancer has been modeled by combining 3D bioprinting with microfluidics to generate a metastasis-on-a-chip platform [54]. In this platform, HCT-116 cells represent colon cancer, INT-407 represent healthy intestinal epithelial cells, and HepG2 cells represent liver cells. This model confirmed cell migration from metastatic tumor foci from the gut construct to the liver construct within the microfluidic chip. The setup was later manipulated to include chemical modulation of the hydrogel mechanical properties and administration of chemotherapeutic drugs to evaluate the effects of these parameters on invasive tumor migration.

An alveolar bone model combined with an oral mucosa model was also fabricated by combining oral squamous cell carcinoma (OSCC) cells with oral keratinocytes, oral fibroblasts, and alveolar osteoblasts [69]. The construct consisted of a tri-layered structure of epithelial tissue, connective tissue, and bone layers, thereby replicating normal oral tissue architecture, and the model was used to study bone invasion by oral cancer, proving its usefulness.

Each of these studies used a single type of cancer, so these results emphasize that tremendous potential exists in bioprinting models using other types of cancer cells. This would allow comparisons between different models according to the parameters to be evaluated and it would bring us closer to their application in personalized medicine.

3.4. Complex models that include vasculature

Tumor vascularization is a key process in cancer metastasis. During this process, tumor cells undergo an epithelial to mesenchymal transition and they might enter the vascular system to produce metastases distant from the primary tumor site [108]. As mentioned earlier, the complexity of a tumor model goes hand in hand with the different cell types coexisting within the construct. However, fabrication of large tumor models requires that vasculature be integrated within the structure. This has been partially achieved by creating constructs with hollow channels with, for example, a honeycomb multilayered array generated by stereolithography, where the hollow channels were used to perfuse the model with culture medium [67]. Nevertheless, recent advances have managed to incorporate endothelial cells, either alone or inside the prefabricated microchannels, to establish more realistic vascular networks.

Some researchers have attempted to reproduce vascularization in breast cancer models by adding endothelial cells within the constructs and by combining hydrogels with microfluidics to recreate the tumor-vascular interface [76]. This kind of experiment utilized a microfluidic device comprising two microchannels interconnected by an ECM hydrogel. The MDA231 breast carcinoma cells were seeded in the presence or absence of macrophages (RAW264.7) in one channel, while MVEC or HUVEC cells were seeded in the other channel to generate a vascularized tumor model to study the endothelial barrier function [76]. Other researchers have combined adipocytes, mammary fibroblasts and endothelial cells to produce self-standing structures that show interactions between stromal and cancer cells and the formation of endothelial networks [78]. Still others have attempted direct bioprinting of breast cancer spheroids in co-culture with HUVECs to create models that rapidly replicate the tumor microenvironment and can be almost immediately used for drug testing [70].

A better structured and vascularized 3D cancer model was created by fabricating breast cancer microtumors by encapsulating MCF-7 cells in collagen microcapsules and then using them as building blocks for assembly in a PDMS-glass microfluidic perfusion device. After placement of the building blocks inside the device, a collagen solution containing HUVECs and ADMSCs was added [109]. After four days of culture, the HUVECs assembled into vasculature with a lumen and surrounded the microtumors.

A different approach is to create a single microtumor surrounded by stromal bioink. One research group tuned different hydrogels to alter the tensile strength and rigidity for the biofabricated tissue but then eliminated this matrix to leave a purely cellular structure in subsequent culture [34]. They used breast cancer cells (MCF-7), primary human mammary fibroblasts, subcutaneous preadipocytes that were differentiated after bioprinting, and HUVECs. This bioprinted structure showed its own ECM deposition and maturation, as well as a close interaction between tumor and stromal cells and the self-arrangement of HUVECs into capillary-like networks. This approach was also used to generate pancreatic tumor models with cells obtained directly from patients and using human primary pancreatic stellate cells as stromal cells [34].

More complex and realistic cancer models can be created by adding signaling molecules, such as growth factors, into the mixture. Again, by combining 3D bioprinting with a microfluidic device, a vascularized pulmonary tumor model was generated with HUVECs, fibroblasts, and pulmonary cancer cells (A549). For this study, stromal cells were bioprinted along the whole device, whereas the cancer cells were printed as a droplet on one side of a vascular channel. VEGF and EGF capsules of increasing concentrations were placed at different sides of the vascular channel, and their contents were released by infrared radiation. This setup created two growth factor gradients that guided tumor

intravasation and *in vitro* metastasis [61].

This technology is promising for application in personalized medicine. For example, glioblastoma-on-a-chip models have been elaborated to test drug candidates and identify the best drug combination according to each patient's needs. For this, patient-derived GBM cells were co-cultured with HUVECs in a brain decellularized ECM, so that GBM cells grew in the middle and HUVECs surrounded them [72]. This model successfully recapitulated the structural, biophysical, and biochemical properties of native tumors, and showed patient-specific resistances to the treatments applied. Simpler vascularized GBM models have also been developed by separately bioprinting a blood vessel layer consisting of HUVECs and lung fibroblasts (LFs) and then seeding preformed U87 MG multicellular tumor spheroids [90].

A vascularized hepatocellular carcinoma model was also generated by combining 3D bioprinting and microfluidics. In this case, the human SMMC-27721 cell line was co-cultured with HUVECs that had been transfected with simian virus 40T antigen (transformation that had the objective of immortalizing these endothelial cells [110]); peripheral blood mononuclear cells were also added [79]. The microfluidic chip consisted of two channels and an array of microstructures communicating them. Hepatoma cells were seeded as spheroids in one channel and HUVECs were seeded as individual cells in the other channel. This array was later used for pharmacodynamic testing.

3.5. Characterization of 3D bioprinted constructs

Once a tumor model is fabricated by 3D bioprinting, several methods are available to characterize the construct (Fig. 5). A point worth mentioning is that none of the following methods on its own is sufficient for correct characterization of a bioprinted tumor. All of them provide valuable information about the three-dimensional structure of the cells within the construct and about their cancerous phenotype according to their marker expressions.

3.5.1. Mechanical testing

Mechanical characterization (Fig. 5A) of 3D structures can be made by dynamic mechanical analysis (DMA) or atomic force microscopy (AFM) nanoindentation. DMA measures the average mechanical properties of a material—or printed tumor, in this case—without differentiating between different regions of the construct. By contrast, AFM nanoindentation measures the mechanical properties, such as the hardness, elasticity, and plasticity index of a material. The main advantage of nanoindentation over DMA is that AFM provides possibility to measure heterogeneous constructs and to identify the mechanical characteristics of specific zones within the construct.

This assessment for bioprinted tumors is not very common, and only a few reports mention mechanical analysis of the 3D constructs after bioprinting and crosslinking. When this assessment is performed, it focuses on measuring the general structural stiffness related to the hydrogels used and their degree of crosslinking.

After printing, 3D constructs are frequently analyzed to assess their stiffness through compression tests (using DMA) or AFM [50,66,113]. Different factors influence matrix stiffness; for example, a proportional relationship exists between the polymer concentration in the hydrogel and the resulting stiffness, which is also affected by the crosslinking degree. For instance, for alginate hydrogels, the use of high

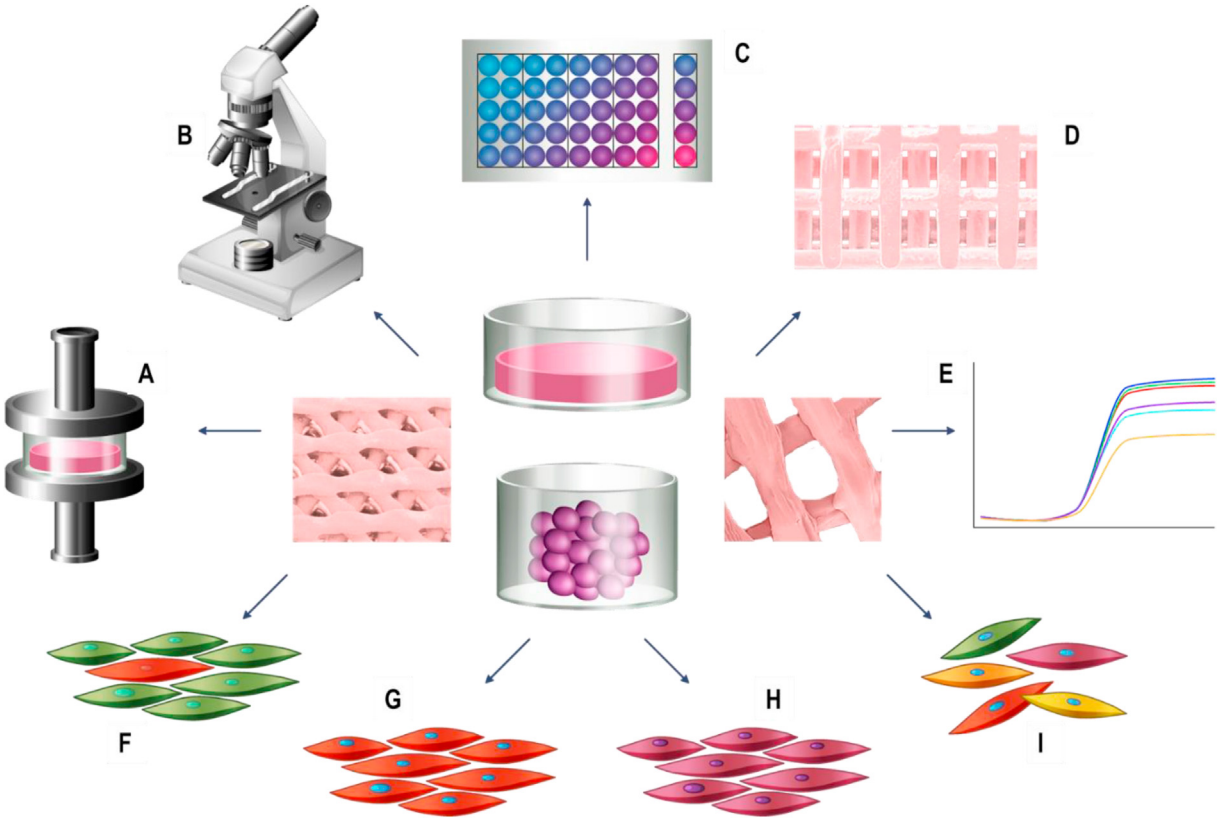

Fig. 5. Characterization techniques used for 3D bioprinted tumor models. Bioprinted tumors pass through several characterization stages. Mechanical assessment (A) can be performed with dynamic mechanical analysis (DMA) or atomic force microscopy (AFM) nanoindentation to assess the matrix stiffness. Microscopy techniques (B) involve confocal, optical, scanning electron microscopy (SEM) and fluorescence. Metabolic activity is measured with colorimetric methods like AlamarBlue, MTS or PrestoBlue (C). Visual assessment involves analysis of photographic images to measure diameters and lengths of the bioprinted constructs (D). Quantitative measurements of representative markers are made by qPCR (E). Cell survival can be assessed with Live/Dead stainings (F). Cell morphology and distribution in space can be observed with fluorescence stainings like Actin/DAPI (G), histological stainings like hematoxylin and eosin (H&E) (H), and immunofluorescence stainings (I).

concentrations of $CaCl_2$ as crosslinking solutions increases the matrix stiffness [50]. In the case of hydrogels that are crosslinkable by UV light, a long exposure time can also cause a high stiffness, thereby limiting oxygen and nutrient diffusion [113]. Exposure to a chemotherapeutic agent can also change the matrix stiffness of a heterogeneous construct with different cell types, as assessed by AFM nanoindentation [63].

Crosslinking different sections of the same construct at different times introduces the possibility of creating matrices with tuned stiffness [64,66]. These findings support the concept that matrix stiffness is important for cell spreading and elongation [75], as well as for angiogenesis, metalloproteinase expression, tumor cell migration, and metastasis [70,109].

Mechanical analysis of 3D bioprinted tumor models must be applied more broadly in the future to evaluate the effects of different hydrogels or composites or the addition of other factors on the microarchitecture and encapsulated cell behavior. Assessment of the matrix stiffness at the beginning of any experiment will allow prediction of how the cells are going to populate the scaffold and whether a correct nutrient and oxygen transport will be established inside the construct.

3.5.2. Cell viability

Upon fabricating a 3D construct, analysis must be performed to confirm that the cells have survived the bioprinting process. This can easily be done using any Live/Dead cell staining kit [50–53,56,59,60,63,64,70]. Live/Dead stains (Fig. 5F) are based on cell membrane integrity and enzymatic activity and have been widely used to assess cell viability in mammalian cell cultures. Even for cells within 3D structures, these assays give good quality results.

Live/Dead stains use calcein acetoxymethyl ester (calcein-AM), a highly lipophilic and cell-permeable compound. Calcein-AM is not fluorescent on its own, but when cleaved by cellular esterases it emits a green fluorescence. The other commonly used stain is propidium iodide (PI), which is not cell membrane permeable and only passes through the membranes of dead cells, where it intercalates with DNA and emits a red fluorescence [114]. This assay has the advantage of respecting cell integrity, but the protocol must be adapted to work inside a 3D structure.

3.5.3. Proliferation

Proliferation over time can be measured in a quantitative manner using metabolic activity assays (Fig. 5C), such as AlamarBlue [62], PrestoBlue, the MTS assay [62,65], and others.

The MTS assay is based in a tetrazolium reagent that is directly soluble in culture medium. Since MTS (3-(4,5-dimethylthiazol-2-yl)-5-(3-carboxymethoxyphenyl)-2-(4-sulfophenyl)-2H-tetrazolium) is a negatively charged compound, it must be used with an intermediate electron acceptor to facilitate the reduction of the tetrazolium into a colored formazan product [115]. Alamar Blue and Presto Blue incorporate resazurin, a redox indicator that changes in response to chemical reduction of the growth medium resulting from cell growth. It is a blue non-fluorescent dye that is reduced to a pink-colored, highly fluorescent resorufin [116]. These assays are useful for measuring cell proliferation in 3D bioprinted constructs and to assess the decrease in cell metabolism caused by the addition of chemotherapeutic agents. The main advantage of these last two methods (Alamar Blue and Presto Blue) is that the cells need not be sacrificed after the application of the dyes, and several measurements can be performed in a single construct over time.

Despite these advantages, an important point to remember is that these kits were originally designed for use in 2D cell cultures, so protocols must be adapted to use them in 3D constructs by either increasing concentrations or reaction times.

3.5.4. 3D structure

The structural assessment of a 3D construct can be performed at different levels, with each level providing unique information about the shape, resolution, fidelity, cell distribution, morphology, and even phenotype. The evaluation as a whole provides an insight into the microarchitecture of the tumor model. Different stainings and microscopy techniques have been used to evaluate the structure of 3D bioprinted tumor models.

The assessment usually starts at the centimeter and millimeter scale by photography and image analysis (Fig. 5D). This serves to assess the resolution and fidelity of 3D bioprinted structures, and parameters such as filament diameter can be measured and compared [73]. A common tool for image analysis is the Image J software [64,72,117].

The construct can then be observed and topographically characterized by SEM, which is useful for observing certain details, like the surface texture [77]. SEM analysis permits the direct observation of the cell–ECM and cell–cell interaction, as well as cell morphology and attachment to the structure with high resolution [49,55,56,69,77,84].

Confocal microscopy (Fig. 5B) can be used for preliminary observations of the 3D structure and to learn if cells are occupying the whole scaffold [75,85,113]. For further structural characterization, confocal microscopy can be combined with fluorescence stainings, like Actin/-DAPI (Fig. 5G), to observe cell morphology. The nuclei are stained with DAPI (4′,6-diamidino-2-phenylindole), whereas, to stain the cytoskeleton, the most common target is F-actin, although staining β-tubulin III, GFAP, and vimentin is also possible [49,64]. This staining serves to confirm the presence of cells within the construct and to corroborate the expected shape of each cell type [56,63,64,68,72].

Finally, histological staining (Fig. 5H) provides additionally observations of the internal structures according to the presence of proteins and does not require a fluorescence microscope [50,69]. It also can reveal the distribution of different cell types that are co-cultured in the same structure [68,72,84].

For all these approaches, image analysis is a tool for quantifying parameters such as cell morphological changes [85,118], proliferation, and migration [64]. Imaging tools provide numerical information on cell numbers and morphology, thereby giving reliable data regarding these factors and their effects on the 3D structure. The information provided by these analyses confirms whether cells in co-culture retain their phenotype and whether the model is truly recapitulating the tumor microenvironment.

3.5.5. Gene and protein expression

Bioprinted tumor models, just as real tumors, should be dynamic entities. This means that they should display a differential expression of relevant markers with time. For this reason, observing and measuring these changes at different time points is critical for knowing what is happening within the construct. Two main techniques are used to assess the expression of relevant markers. One is immunofluorescence staining (Fig. 5I), which shows where the markers are being expressed. The other is quantitative PCR (qPCR), which provides a quantitative value for that expression (Fig. 5E).

Immunofluorescence staining targets the expressed proteins, so it provides qualitative information about the expression of proteins with specific cell localizations or that represent a specific phenotype. The main advantage of this type of staining is that it can be performed *in situ*, meaning that even when the tumor model construct must be sacrificed, there is no need to dissociate it.

One of the main uses of immunofluorescence is for the observation of specific protein expression within the cells. When targeting CD31, this technique helps identify the endothelial network [63,72,113,119] and can reveal the vascularization potential by the expression of VEGF [49]. When constructs are not vascularized, proliferating and hypoxic cells can be identified with Ki67 and pimonidazole [34,72], respectively.

The cancerous phenotype of epithelial cells in different tissues can be confirmed using markers like CK5, CK8, nestin, E-cadherin, caspase 3, and SOX2 [63,68]. Distinguishing between different cell populations within a co-culture 3D construct is also possible [54,63,107,120]. Cell-cell interactions can also be assessed with immunostaining by observing cell adhesion markers like ZO-1, LOX, N-cadherin, and collagen [54,63,111], as well as gap junctions [107]. Lastly, confirmation of an *in vivo*-like phenotype can be made by staining for β-catenin,

vinculin, and PCNA [56], and the migration and invasion potential can be confirmed by staining for MMP2, MMP9, and vimentin [54,79,111].

For deeper analyses and phenotype characterization, performing qPCR or RT-qPCR is worthwhile for the quantitative assessment of specific markers that represent stemness, invasion potential, malignancy, etc. These techniques are based on RNA rather than protein, and they complement immunofluorescence results. Unlike immunostaining, however, these analyses cannot be performed *in situ*. The matrix where cells are embedded must be disassembled to allow disruption of the cell membranes and release of mRNA.

Some researchers also use qPCR to assess neural stem/progenitor cell markers, such as CD133 and nestin [55,59,121]. CD133 is a membrane glycoprotein [122] and nestin is a cytoskeletal intermediate filament protein [121]. Matrix metalloproteases (MMPs) have also been measured by qPCR. These are key enzymes responsible for the ECM breakdown required to allow cancer cell migration [123]. These MMPs are usually overexpressed in tumor tissues compared to normal adjacent tissues [12]. MMP1 [72], MMP2 [53,72], MMP9 [53,72,84], and other ECM-remodeling proteins, like protein tyrosine kinase 2 (PTK2) and fibronectin [72], have also been associated with drug resistance [84]. Another overexpressed marker related to drug resistance is MGMT [84], which is a DNA adduct repair protein [124]. Other genes related to multidrug resistance are the ATP binding cassettes (ABCC1, ABCB1, and ABCG1) [63].

Genes associated with tumor aggressiveness and progression [34,125], like hypoxia marker HIF-1α [59,63], vimentin [85], N-cadherin [61], collagen family (COL1A1, COL1A2, COL4A1), osteopontin (OP), osteonectin (ON) and osteocalcin (OC) [69], have also been measured.

The expression of pro-angiogenic factors, as sign of vascularization and malignancy, can also be measured by qPCR. High expressions of VEGFA and IL8 [72], as well as VEGFR2 [59], have been associated with malignancy. If endothelial cells are present in the tumor model, the expression of cell junction molecules (PECAM1, CDH5 and TJP1 [72]) and endothelial differentiation markers (CD31 [59]) can also be measured.

According to the previous reports, the combined use of immunofluorescence staining and qPCR has allowed an integral evaluation of the cells encapsulated in a 3D bioprinted tumor model. The correct choice of markers has permitted measurements of the stemness and the angiogenic and metastatic potential of cancer cells. Application of this knowledge to biopsy-derived tumor cell constructs would possibly provide better treatments and improved prognoses for cancer patients.

4. Applications

Bioprinting of solid tumors is gaining interest. Current 3D bioprinting platforms have allowed the incorporation of multiple cell types, diverse ECM materials, and spatial and temporal introduction of signaling molecules and growth factors [27]. These advances have broadened the application potential of these models.

4.1. Tumor biology, invasion, migration, and metastasis

Understanding tumor biology is providing the possibility of getting to the core of cancer as a multifactorial disease. However, this increased understanding is also bringing about a realization that tumor heterogeneity caused by subtle genetic variations is the main cause of drug inefficacy in some patients and therefore dictates their prognosis. The use of 3D bioprinting to generate tumor models now allows the study of tumor biology at both the molecular and physiological levels.

4.1.1. Breast cancer

The wide study of breast cancer in bioprinted models has evolved from simple evaluation of cell migration potential and how it is affected by the hydrogel matrix to the interaction between breast cancer cells and immune or stromal cells and its effect on drug responses.

A breast cancer model comprising normal breast epithelial cells (HMLE) and Twist-transformed cells (HMLET) used PEGDA scaffolds to tune the elastic moduli and microstructure of 3D constructs [66]. The findings indicated that hydrogel stiffness and Twist transformation had a significant effect on cell migration. HMLET cells were able to migrate farther and faster in stiffer hydrogel, whereas HMLE cells migrated more efficiently in a softer hydrogel matrix [66]. MDA-MB-231 or MCF-7 cells have also been combined with MCF10A cells to assess migration. In this case, 3D constructs were fabricated by a two-step photolithography technique, which allowed the precise location of cells encapsulated in circular constructs next to a low stiffness matrix. Cells were tracked in real time, and MDA-MB-231 cells were able to migrate and invade the surrounding matrix, while MCF7 and MCF10A formed spheroids that remained confined in their original position. The MDA-MB-231 cells also displayed 3D protrusions not seen in the MCF7 and MCF10A clusters [64]. The MDA-MB-231 cells were also incorporated in a model with IMR-90 CAFs. After 7 days of culture, the MDA-MB-231 cells formed tumor spheroids (Fig. 6A), which grew and increased in number over time, and after approximately 15 days, the CAFs had migrated through the hydrogel matrix and infiltrated the breast cancer spheroids [57]. These models proved that hydrogel matrices with tunable stiffness and architecture are suitable for evaluation of tumor cell migration. A different approach to study migration and metastasis was developed by culturing MDA-MB-231 cells in a GelMA matrix together with lymphatic endothelial cells (LECs) in pre-engineered vessels [105]. The LECs sprouted into the surrounding hydrogel matrix, thereby establishing lymphangiogenesis as a potential therapeutic cancer target.

A customized bioprinting platform was built to print chimeric organoids comprising normal mammary epithelial cells (MCF-12A) and tumorigenic MDA-MB-468 or MCF-7 cells (Fig. 6B). The system successfully generated tumoroid arrays, and the cells in these chimeric structures showed a significant increase in levels of 5-hydroxymethylcytosine, an intermediary in gene demethylation. This was attributed to the surrounding normal mammary microenvironment, which can mediate epigenetic alterations in cancer cells and cause them to revert to their tumorigenic phenotype [68].

Different breast cancer models have created increasingly more complex structures to assess bone metastasis. The use of nano hydroxyapatites (nHA) to coat PLA scaffolds has enhanced the metabolic activity of human bone marrow derived MSCs and breast cancer cells (MDA-MB-231) [77]. In a similar model, nHA were added to PEGDA/PEG resins and used to build a geometrically optimized matrix for co-culture of MDA-MB-231 cells with bone marrow MSCs. Breast cancer cells in this experimental setup exhibited spheroid morphology, whereas the MSCs grew as a monolayer within the bone matrix [65]. Composites of nHA and GelMA have also been used to fabricate a bone matrix consisting of fetal osteoblasts and human bone marrow MSCs. Within this matrix, the growth of MDA-MB-231 cells was enhanced by the presence of MSCs and osteoblasts, while the proliferation of these cell populations and their alkaline phosphatase activity were inhibited by the co-culture with breast cancer cells [62]. All these models show promise for studying breast cancer bone metastasis.

Other breast cancer models have combined MDA-MB-231 cells with murine macrophages (RAW 264.7) to analyze the paracrine loop between these cell types (Fig. 6C). For these experiments, two bioinks, one comprising tumor cells and the other one comprising macrophages, were coextruded to form fibers. A Pearson correlation was then used as a metric of the degree of dispersion between the two cell populations. In this matter, a high positive correlation factor corresponds to a well-mixed and heterogeneous cell population, while a negative correlation factor corresponds to separation of the two cell populations. The results showed that tumor cells attract macrophages and that the shape of the fibers (straight, serpentine, helically packed) influences the interactions between cell types and, therefore, their migration potential [58].

Breast cancer models have evolved more rapidly and efficiently than other types of cancer models. The exhaustive research on these models

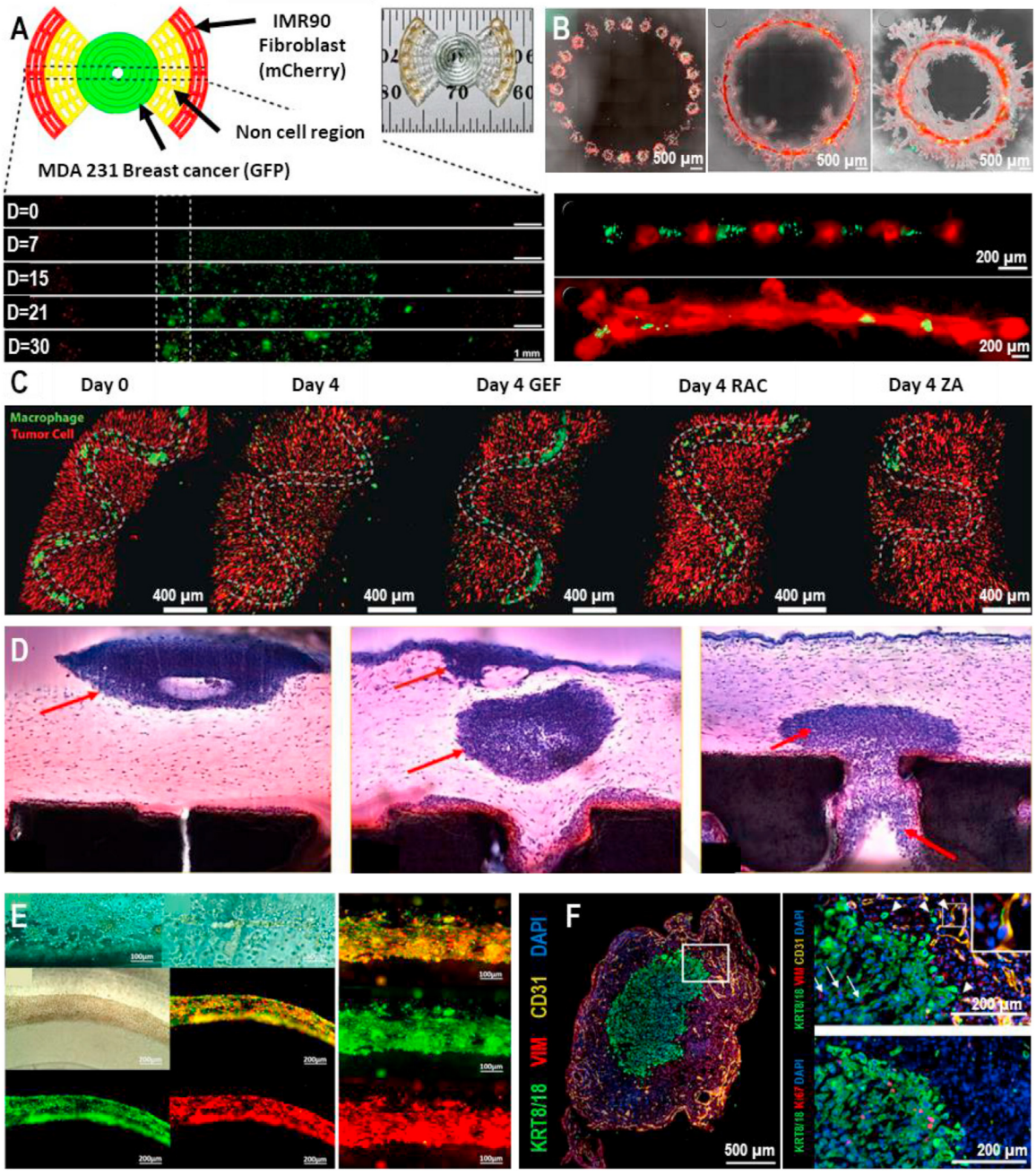

Fig. 6. 3D bioprinted tumor models that recapitulate cancer migration and invasion. (A) Multicellular tumor spheroid formation within a 3D bioprinted *in vitro* model consisting of IMR-90 fibroblasts and MDA-MB-231 breast cancer cells. The image depicts the CAD model and a bioprinted sample in which IMR-90-mCherry (red) fibroblasts were encapsulated in the outer parts of the construct and MDA-MB-231-GFP (green) breast cancer cells were encapsulated in the middle part of the construct, leaving an acellular region between the two cell types. Cells were tracked on days 0, 7, 15, 21, and 30 to determine how both cell types migrate toward each other. Adapted from Ref. [57] (B) Top: Chimeric organoid generated by printing MCF-12A normal mammary epithelial cells (red) and MDA-MB-468 breast cancer cells (green) cells at days 3, 7, and 21 with a 500 µm spacing in a circular pattern (Scale bar: 500 µm). Bottom: When alternating MCF-12A (red) and MDA-MB-468 cells (green) with a 300 µm spacing, migration and incorporation into an organoid is observed (Scale bars: 200 µm). Adapted from Ref. [68]. (C) Fluorescence imaging of 3D bioprinted fibers showing macrophages (green), tumor cells (red), and the location of a hollow inner channel indicated in dotted lines. At the beginning of the experiment, macrophages were exclusively located in the hollow channels of the fibers, but after 4 days of culture, they became interspersed among the tumor cells. This effect was inhibited by treatment with Gefitinib, a Rac1 inhibitor, and zoledronic acid, causing an impairment of migration and the permanence of most macrophages in the channel (Scale bar: 400 µm). Adapted with permission from Ref. [58]. (D) H&E staining of a 3D bioprinted model recapitulating bone invasion of oral cancer and showing tumor spheroids invading the mouth epithelium (left); the epithelium and connective tissue (middle); and connective tissue layer in direct contact with the bone (right). Adapted with permission from Ref. [69] (E) Coaxially extruded fibers comprising glioma stem cells and MSCs that fuse into flakes and strands after migration. The interaction between cell types was observed at days 3 (left) and 7 (right). Adapted from Ref. [50]. (F) Bioprinted pancreatic cancer model containing patient-derived cancer cells surrounded by pancreatic stellate cells and HUVECs (Scale bar: 500 µm). After 7 days of culture, isolated stromal cells, indicated by arrows, are found within the cancer region. The arrowheads show cancer cells forming intimate connections with endothelial cells in the stromal region (Scale bar: 200 µm). Adapted with permission from Refs. [34]. (For interpretation of the references to color in this figure legend, the reader is referred to the Web version of this article.)

has managed to involve and assess the presence of immune, stromal, MSC, and endothelial cells. Furthermore, more complex processes like bone metastasis have been effectively recapitulated thanks to breast cancer bioprinting.

4.1.2. Glioblastoma

Cancer cells from different origins, ranging from cell lines to patient-derived biopsies, have been employed for the fabrication of glioblastoma models. These models have enabled the evaluation of several variables of glioblastoma tumors.

Measuring markers by immunostaining or qPCR has allowed the use of single-cell GBM models for the study of bioprinted cells stemness and differentiation potential [49], as well as the EMT and *in vivo* tumorigenicity [55]. Stemness has been evaluated by nestin and CD133 expression [126], while differentiation potential has been assessed by glial fibrillary acidic protein and β-tubulin III expression [127,128]. GBM models comprising only cancer cells have allowed evaluation of the effect of 3D bioprinting on cell viability and proliferation, while cells grown into spheroids have pushed the boundaries of the hydrogel scaffold and show a behavior similar to *in vivo* tumor growth [60].

GBM 3D constructs comprising GSCs have also been compared with suspension cultures. In this case, GSCs in 3D scaffolds gradually formed spheroids, while cells in suspension showed abnormal growth and cell death. Proliferation was dramatically increased in the first five days of suspension culture but decreased rapidly afterward. By contrast, cells in the 3D scaffold gradually proliferated and reached a peak in ten days, when their proliferation rate became stable and higher than that of cells in suspension. The expression of the CD133 stemness marker was also ~74 fold higher in 3D scaffolds, as confirmed by flow cytometry, where the $CD133^{+}$ cell phenotype was ~32% in 3D culture and ~19% in suspension culture [59].

For simple GBM representation, co-extruded fibers comprising glioma stem cells (GSC23) and MSCs were used to study the interaction between these two cell types and the intrinsic tumor biology (Fig. 6E). GFP-expressing MSCs and RFP-expressing GSCs were bioprinted into the core of the fiber. After 7 days, they displayed stretching and integration into fibers. Higher expression of the stem cell biomarker nestin, along with the MSC biomarkers CD44 and vimentin, was observed in coaxially bioprinted tumor fibers than in xenografted tumors and cell-laden hydrogel constructs, and this expression was comparable to the observed in GBM tissues. Cell fusion between GSCs and MSCs was also assessed with a CRE-LOXP system. First, the GSCs were transfected with LOXP-STOP-LOXP-RFP genes and the MSCs with CRE recombinase. When fused together, the cells started transcribing and expressing RFP, which was assessed by qRT-PCR and confocal microscopy, whereas the control group did not show RFP expression [50].

A GBM model also made of coextruded fibers was generated with or without GSC23 cells (determined as G/U and U, respectively) in the shell and U118 glioma cell line in the core of the fiber. U118 cells proliferated to form cell aggregates with an increased cell–cell and cell–ECM interaction. The expression of MMP2, MMP9, VEGFR2, and O6-methylguanine-DNA methyltransferase (MGMT), which are all markers related to tumor invasion and drug resistance, was higher in the G/U fibers than in the U fibers [84]. Glioma cell (U118) invasion in real time into iPSC-derived human neural progenitor spheroids was also assessed using cell-tracking dyes and 3D laser scanning confocal microscopy, with results confirmed by conventional cryosectioning, to introduce an appropriate model that mimicked the heterogeneity of tumors to examine invasion by different cell lines [107].

Two more GBM models were bioprinted to verify the recapitulation of the tumor microenvironment. One used U87-MG cells, WI-38 non-immortalized fibroblasts, and MM6 macrophages. The other one used GSCs, patient derived GASCs and human microglia. GSCs did not show any loss in stemness marker expression, even after growth factor withdrawal [75].

GBM has also been modeled by bioprinting of murine micro-tissues, consisting of clusters of GL261 glioblastoma cells and RAW264.7 macrophages, to study the paracrine and juxtacrine signaling between these cell types. First, the larger part, comprising macrophages, was printed with an empty cavity. Subsequently, the cavity was filled with GL261 bioink. Macrophages in this model, when compared to a 2D model, had an increased expression of MMP2, MMP9, and other crucial genes known to be overexpressed in glioblastoma-associated macrophages (GAMs). The GL261 cells also displayed a higher expression of GBM-specific markers, such as glial fibrillary acidic protein and chitinase like 1, compared to a 2D monolayer culture. The findings support the idea that GBM cells can recruit macrophages and turn them into GAMs, while the GAMs induce GL261 invasiveness in these glioblastoma/macrophage tissue constructs [56].

GBM modeling is beginning to cross the frontiers into personalized medicine. Patient-derived cells were co-printed with HUVEC cells in a brain decellularized ECM (BdECM) hydrogel to create Glioblastoma-on-a-chip constructs, with tumor cells in the middle and endothelial cells surrounding them. Cell viability and relevant gene expression was compared with constructs that used collagen hydrogel, and both parameters were significantly higher in BdECM. Immunostaining with pimonidazole for hypoxic cells and Ki67 for proliferating cells was performed in the GBM chips to confirm native GBM hypoxic conditions. The GBM cells were also observed to begin invading the endothelial region of the construct, and HUVEC cells started invading the tumor region of the construct [72].

The EMT, *in vivo* tumorigenesis, stemness, differentiation potential, cell fusion, ECM remodeling potential, paracrine and juxtacrine signaling are only a few of the several variables that have been successfully assessed in 3D bioprinted glioblastomas. This information gives us a broad insights into how evolved these models already are, but it also shows some opportunity areas that should be addressed in the future, such as the inclusion of endothelial cells in models that already have immune or stromal cells.

4.1.3. Ovarian and cervical cancer

Besides breast cancer, ovarian and cervical tumors are types of cancer that also afflict women around the world. These cancers are not as prevalent as breast cancer, but some bioprinted models have already been reported.

For ovarian cancer models, OVCAR5 cells printed with MRC-5 fibroblasts formed 3D acini, and both cell populations showed co-migration after a week [71]. Fibroblasts that were closer to OVCAR5 cells were able to significantly increase the size of the 3D micronodules, thereby emphasizing the relevance of the spatial location of stromal cells in tumors [95].

HeLa cells in a 3D cervical cancer tumor-like construct showed spheroid morphology, in contrast with the elongated shape of HeLa cells in 2D culture. They also showed a higher proliferation and elevated metalloprotease expression, indicating that this model closely mimics the *in vivo* behavior of cervical cancer [89]. The 3D bioprinted HeLa cells have also shown a fibroblast-like spindle morphology after supplementation with TGF-β, indicating operation of the EMT, and these results were confirmed by the up-regulation of mesenchymal markers like snail, vimentin, and N-cadherin [85].

Cancer cell migration has also been evaluated in a cervical cancer model comprising HeLa and 10T1/2 cells. In this model, the cells were seeded in a honeycomb branched structure that was 3D printed in a micro-chip. These structures functioned as geometric cues that affected the area and migration speed of the HeLa cells, but not of the 10T1/2 cells, thereby providing clues for a better understanding of cancer biology and metastasis [67].

Ovarian and cervical tumor models have not evolved as quickly as those for breast cancer. As a perspective, we expect that future bioprinted models will include different cancer cell lines, as well as other types of cells besides fibroblasts. With these improvements, researchers will be able to provide better *in vitro* models for studying cervical and ovarian cancer biology and for evaluating drug responses.

4.1.4. Lung cancer

Lung cancer is the most prevalent and lethal type of cancer worldwide. Nevertheless, insufficient numbers of bioprinted models have been reported to date. The current models have focused on evaluating the invasion and migration ability of the cancer cells within the constructs.

One 3D lung cancer model used bioprinted cells, and the constructs were later dissociated to retrieve the cells and perform invasion and migration experiments. Cell invasion potential was measured by metalloprotease expression, while actual migration was evaluated with a transwell assay and by a scratch test, where the rate of gap coverage was correlated with the migration capacity of the cells. Both A549 and 95-D cells from the 3D constructs had higher invasion and migration capability than their counterparts from 2D culture [53].

Recently, a more complex pulmonary cancer model also included growth factors to direct cell migration of both tumor and endothelial cells. A microchip was designed with a central microchannel containing endothelial cells with two adjacent chambers with programmable capsules of different sizes to create growth factor gradients. Both chambers were filled with fibroblasts; the left channel generated a VEGF gradient while the right chamber originated an EGF gradient after the capsules were ruptured with infrared radiation. A tumor droplet of A549 cells was then placed in the left chamber. Tumor cell migration was effectively guided by the EGF gradients, while vascularization was guided by VEGF gradients, as observed by fluorescence microscopy [61]. This proved to be a useful model for studying tumor cell intravasation and posterior metastasis.

The representation of lung cancer through 3D bioprinting is complicated by the nature of the lungs, which are in direct contact with air. Self-standing 3D bioprinted models have not yet reached the capacity to sustain cell growth while being in direct contact with the atmosphere, so this represents an opportunity area for fabricating better lung cancer models.

4.1.5. Other cancer models

Other types of cancer that have been successfully represented with 3D bioprinting techniques include colon, oral, and pancreatic cancers. These models have focused in recapitulating invasion, migration, and metastasis phenomena.

Regarding migration and metastasis, a colon cancer model was elaborated using 3D bioprinting to fabricate a gut organoid and a liver organoid in a chip to create a metastasis-on-a-chip model. The gut construct contained Int-407 intestine epithelial cells and either SW480 or HCT-116 colon cancer cells, whereas the liver construct contained only HepG2 cells. Culture medium flowed from the gut to the liver, and after 14 days of culture, metastatic HCT-116 cells started disseminating from the gut construct into the circulating medium. Two or three days later, metastatic cells started invading the liver construct via multicellular aggregates. By contrast, SW480 cells were able to colonize the gut construct were unable to metastasize to the liver construct [54].

A remarkable application of 3D bioprinting for cancer studies was the fabrication of a multi-layered model consisting of human alveolar bone combined with oral mucosa. This construct was used to incorporate oral squamous cell carcinoma (OSCC) spheroids at different levels to represent different stages of oral cancer (Fig. 6D). The structure was evaluated using histochemistry and was confirmed to replicate normal oral tissue architecture. OSCC spheroids were also found at three depths of the structure, including the supra- and sub-epithelial levels and the connective tissue-bone interface, thereby identifying this as a great model for oral cancer invasion [69].

Similarly, a pancreatic ductal adenocarcinoma model was bioprinted using a patient-derived pancreatic cell line, HUVEC cells, and normal human primary pancreatic stellate cells (PSCs). The pancreatic cancer cells formed tumor tissues surrounded by an extensive network of PSCs and HUVECs. Isolated stromal cells were observed within the cancer region and, correspondingly, cancer cells were observed connected with endothelial cells (Fig. 6F). The cancer cells retained their proliferative capacity, as observed by Ki67 staining, and implantation of the bioprinted tissues into mice led to tumor formation *in vivo*. Cytokeratin-expressing pancreatic cancer cells also kept an ordered structure and displayed a cuboidal organization surrounding a lumen in some regions, hence recapitulating the *in vivo* spatial organization [34].

Among these types of cancer, colon cancer is the most prevalent and one of the hardest to represent, not only because of the different cell types, but due to the interactions between intestine epithelial cells and the gut bacteria. One colon cancer model has resulted in the most successful representation of *in vitro* metastasis to a close organ. The most complex model was the one representing oral cancer thanks to the several layers it comprised. The pancreatic cancer model was the most complete because it included stromal and endothelial cells and was also tested for tumor formation *in vivo*.

4.2. Vascularization and endothelial barrier function

The multiple steps of cancer vascularization and metastasis involve tumor–endothelial cell interactions. Intravasation is initially blocked by the endothelial barrier and becomes a rate-limiting step in these processes because it regulates the number of tumor cells that circulate and form secondary tumors (Fig. 7A). Cell-cell communication is a key process during metastasis, as tumor cells cross the tumor microenvironment and enter the blood vessels [76].

The simplest way to assess vascularization potential is by measuring the expression of VEGF or VEGFR in cancer cells, which is possible in single cell models [49] or co-culture models that do not include endothelial cells [84]. A GBM 3D bioprinted model with GSCs was used to evaluate the expression of tumor angiogenesis markers and vascularization potential in comparison with a suspension culture. VEGFA secretion was measured with a sandwich ELISA every 48 h. In suspension cultures, VEGFA increased gradually for seven days and then decreased slowly, whereas in 3D constructs, VEGFA secretion increased steadily and remained stable after 9 days of culture and remained higher than that of the suspension cultures. Furthermore, CD31 and VEGFR2 expression was more than 500-fold and 900-fold higher, respectively, in the 3D constructs than in the suspension cultures [59].

A breast cancer model was developed to study the endothelial barrier function by combining 3D bioprinting with microfluidics (Fig. 7B). In this model, the tumor-vascular interface was recreated by co-culturing MDA-231 and MVEC or HUVEC cells. This model was validated for measuring the temporal response of the endothelium to biochemical factors, as well as the migration of tumor cells across the endothelial surface (Fig. 7C). In the absence of macrophages, only a small portion of tumor cells in contact with the endothelial monolayer were able to intravasate, whereas in the presence of macrophages, a greater percentage of tumor cells managed to intravasate, regardless of the origin of endothelial cells. TNF-α stimulation also promoted an increase in endothelial permeability and intravasation rate [76].

Another breast cancer model was fabricated with microvascular networks and endothelial cells to evaluate the compartmentalization of epithelial components, as well as stromal and adipose elements, which were represented by mammary fibroblasts and adipocytes, respectively. The 3D constructs were histologically and morphologically assessed, and they displayed the formation of endothelial networks, as well as differentiation of MSCs into adipocytes [78].

A pulmonary tumor model generated with growth factor gradients was used to assess angiogenesis (Fig. 7D). A549 cells were seeded on the opposite side of an EGF gradient, while HUVEC cells were seeded inside a microchannel on the opposite side of a VEGF gradient (Fig. 7E). After 12 days of culture, tumor cells had migrated toward the EGF gradient and HUVEC cells had started sprouting toward the VEGF gradient, whereas the tumor showed the onset of vascularization (Fig. 7F). The HUVEC cells also had a higher expression of VEGF and VEGFR in the presence of growth factors than without them [61].

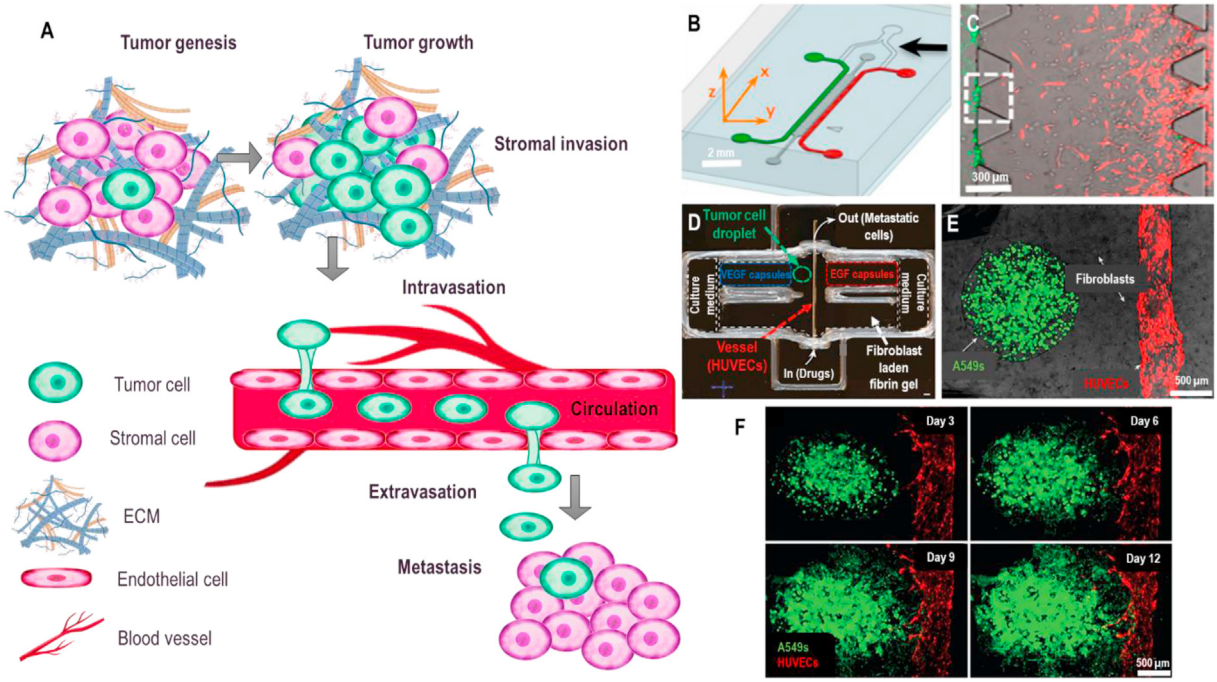

Fig. 7. Modeling the endothelial barrier function through bioprinting of cancer models. Cancer is harder to treat when tumors have caused distant metastases. (A) When a tumor forms and begins to grow, it must sustain its growth by promoting its own vascularization. For this, tumor cells must cross the stromal territory to reach the blood vessels. Once there, and with the help of different cellular interactions, tumor cells can cross the endothelial barrier and enter systemic circulation. The tumor cells can then extravasate the blood vessel in a different location to create a new metastatic tumor. (B) Endothelial channel (green), tumor channel (red), and 3D ECM (dark gray) between the two channels. Black arrow shows the Y junction (Scale bar: 2 mm). (C) Phase contrast image showing cancer cells (red) invading through the ECM (gray) toward the endothelium (green). Dashed square: single 3D ECM hydrogel matrix region (Scale bar: 300 µm). Adapted from Ref. [76]. (D) 3D printed culture chamber for tests of guided tumor cell migration. (E) Representative tumor model before laser-triggered rupture of growth factor capsules (green fluorescence: GFP-expressing A549s, red fluorescence: RFP-expressing HUVECs, bright field: fibroblasts). (F) Fluorescence images of a metastatic model on days 3, 6, 9, and 12, showing that A549 cells approach and enter the vasculature through the stromal region of the gel (green: GFP-expressing A549s; red: RFP-expressing HUVECs). (Scale bar: 500 µm) Adapted with permission from Ref. [61]. (For interpretation of the references to color in this figure legend, the reader is referred to the Web version of this article.)

4.3. Pharmacology testing

Pharmacology testing of anticancer treatments, regardless of their origin, mechanism of action, or even original purpose, has generally been performed in human tumor cell lines grown in monolayers or in animal models, as mentioned earlier. However, the use of 3D bioprinted models for this purpose has increased due to their lower cost, better control, fewer ethical issues, and smaller time consumption. A summary of chemotherapeutics, immunotoxins, and monoclonal antibodies that have been tested in 3D bioprinted tumor models, either for validating the model or for drug screening, is portrayed in Table 2.

4.3.1. Breast cancer

The most common chemotherapeutic agents used to treat breast cancer are doxorubicin, paclitaxel, and 5-fluorouracil (5-FU). These and other drugs have been tested in bioprinted models to validate their utility for drug discovery.

A vascularized breast cancer model comprising adipocytes as stromal cells was used to compare the effects of tamoxifen in 2D culture and 3D constructs. Their results confirmed that cells in the 3D constructs were significantly more resistant to the same dose of tamoxifen as the one applied to cells in 2D culture [78]. A simpler breast cancer model was generated by coextruding fibers with two bioinks, one with MDA-MB-231 cells and the other one with RAW 264.7 macrophages. These fibers were treated with distinct anti-cancer agents, namely Gefitinib (GEF), zoledronic acid (ZA), and a Rac1 inhibitor (RAC). Tracking the cells with confocal fluorescence microscopy revealed that, without treatment, macrophages invaded the tumor region of the fibers. By contrast, in presence of GEF, ZA, and RAC, migration was impaired and most of the macrophages remained within their original location [58]. This provides an insight into the usefulness of this type of model for drug screening against cancer. A model using nHA in PEGDA/PEG resins was used to evaluate the sensitivity of MDA-MB-231 to 5-FU. After three days of treatment, cells in the 3D matrix showed apoptosis but significantly less cytotoxicity than cells in a 2D cell culture [65].

Simple but effective breast cancer spheroids have also been generated by magnetic levitation. This technique can generate spheroids with multiple cell types in different ratios; for example, by combining fibroblasts and breast cancer cells in either 70/30, 50/50, or 30/70 proportions. Fabrication of these spheroids and later exposure to doxorubicin hydrochloride and doxorubicin liposomes (Doxil ®) for 72 h revealed that resistance to both treatments was greater in the 3D construct than in cells in 2D monolayers, but doxorubicin hydrochloride treated constructs showed lower cell viability than Doxil ® treated constructs, regardless of the breast cancer cell-to-fibroblast ratio [111]. Another model used to test doxorubicin was fabricated by 3D bioprinting mammary fibroblasts, subcutaneous preadipocytes, HUVECs, and MCF-7 or MDA-MB-231 cells. After treatment, 3D constructs exhibited a 20-fold LD_{50} compared with cells in 2D co-culture. Another treatment tested in this model was Sunitinib, which inhibits VEGFR in tumors, and it was able to dramatically reduce the endothelial cell networks within 3D bioprinted tissues [34].

A more complex breast cancer model mixed ADMSCs and 21 PT cells to compare their response to doxorubicin with 2D co-cultures. For this purpose, disk-shaped 3D constructs were fabricated with 21 PT cells and surrounded with or without top and bottom layers of ADMSCs hydrogel (Fig. 8I). Measurement of the doxorubicin effect with caspase apoptosis marker expression showed lower expression in the bioprinted constructs

Table 2
Chemotherapeutics and other treatments tested in 3D bioprinted tumor models.

Cancer model	Cell line	Therapeutic	Mechanism of action
Glioblastoma	U118	Temozolomide (TMZ)	Methylates purine bases of DNA [129]
	Patient-derived biopsies		
	U87MG		
	GSCs		
	U87MG	Cisplatin	Crosslinks with purine bases on the DNA [130]
	GL261	Carmustine	Cross-links DNA and RNA, inhibiting DNA synthesis, RNA production and RNA translation [131]
		AS1517499	Stat6 inhibitor [56]
		BLZ945	Inhibits colony stimulating factor 1 (Csf-1r) [56]
Breast	–	Tamoxifen	Blocks estradiol receptor [132]
	MDA-MB-231	Gefitinib	Inhibits EGFR tyrosine kinase [133]
		Zoledronic acid	Inhibits enzymes from the mevalonate pathway [134]
		Rac1 inhibitor	Inhibits Rac1 proto-oncogene [135]
		Doxorubicin	Intercalates into DNA and disrupts topoisomerase–II–mediated DNA repair [136]
		Sunitinib	Inhibits tyrosine kinases [137]
		Paclitaxel	Induces mitotic arrest [138]
		5-FU	Inhibits thymidylate synthase [139]
Hepatoma	HepG2	5-FU	
		Mitomycin	Alkylates DNA, inhibits thioredoxin reductase [140]
	SMMC-7721	Metuzumab	Monoclonal antibody that targets the CD147 [141]
Cervical	HeLa	Paclitaxel	Induces mitotic arrest [138]
		Disulfiram	Inhibits proteasome activity [142]
Ovarian	OVCAR5	Carboplatin	Inhibits DNA replication and transcription [143]
Colon	HCT-116	5-FU	Inhibits thymidylate synthase [139]
Pulmonary	A549	EGF4KDEL	Immunotoxin that blocks EGFR [144]
Pancreatic	Patient-derived cancer cells	Gemcitabine	Incorporates into DNA, inhibiting its synthesis [145]

with stromal cells than in the cancer constructs alone (Fig. 8J). Moreover, inclusion of a LOX inhibitor treatment decreased the ADMSC region stiffness but not the stiffness of the 21 PT region. LOX inhibition also enhanced the doxorubicin sensitivity of cancer cells, faithfully reproducing *in vivo* conditions and thereby providing a suitable model for examining tumor biology and drug screening [63].

Breast cancer spheroids have been directly bioprinted and the effect of paclitaxel concentration assessed in them. The MDA-MB-231 spheroids showed a higher resistance to paclitaxel than did the individual bioprinted cells, and the resistance was hindered when the spheroids were bioprinted together with HUVEC cells [70].

Overall, 3D bioprinted breast cancer models have shown to be more reliable than 2D models, whether for validating models for drug discovery or for evaluating the effect of the presence of other cell types in the response to therapeutic agents.

4.3.2. *Glioblastoma*

TMZ is the gold standard for treating glioblastoma. Therefore, it is the most tested drug in GBM bioprinted models. Carmustine and cisplatin are other chemotherapeutic drugs that have been tested in these models. Immunomodulatory agents have also been tested and compared to a chemotherapy treatment.

GBM single-cell models have been used to assess the effect of TMZ by measuring cell viability after treatment, and the 3D bioprinted models were more resistant to this drug than were 2D cultures [49,55]. A similar study used a GBM-reprogramming cocktail to reprogram GBM cells into early neurons. The ability of the GBM cells to proliferate in the scaffold was impaired, but the display of elongated neurites was not [60]. In the case of co-culture, U118 cells were harvested from G/U and U fibers and reseeded in 2D culture to test their response to different concentrations of TMZ (Fig. 8G). Cell viability after 48 h of treatment showed that U118 cells coming from co-culture fibers were more resistant to increasing TMZ concentrations (Fig. 8H). This was later evaluated by measuring DNA methylation in the MGMT gene promoter, since a higher methylated MGMT gene in tumor cells is equated with lower drug resistance. The results confirmed that the methylation rate was ~18% in G/U U118 cells and ~40% in U U118 cells (Fig. 8H) [84].

TMZ and cisplatin were also tested in 3D bioprinted U87MG cells. Cells in 3D constructs had a twofold increase in IC_{50} values for TMZ compared to 2D cultured cells. In the case of cisplatin, 3D constructs also showed a higher resistance. When macrophages (MM6 or microglia) were incorporated into the constructs, U87MG displayed a decreased drug sensitivity, with a cell survival fraction higher than that without macrophages [75]. Another GBM model that provided a good recapitulation of the TME used a pre-engineered blood vessel layer consisting of fibroblasts and endothelial cells, where multicellular tumor spheroids were later seeded on top. The constructs received either a TMZ alone treatment or TMZ combined with sunitinib, with the second treatment being the most effective in reducing tumor spheroid size and disconnecting vascular networks [90].

Tissue constructs consisting of glioblastoma cells and macrophages were also used for drug screening of chemotherapeutic (carmustine) and immunomodulatory (AS1517499 and BLZ945) drugs for GBM treatment. Three sets of experiments were conducted to study the effects of these therapies on cell growth. Monocultured constructs of either tumor cells (GL261) or macrophages (RAW264.7) were used for the first experiment. The IC_{50} for carmustine in the glioblastoma-macrophage constructs was 581 μm in GL261 cells and 887 μm in RAW264.7 cells. For the second experiment, which used co-cultured glioblastoma-macrophage constructs, tumor pieces were isolated and then treated with carmustine. The growth of tumors isolated from co-cultured glioblastoma-macrophage constructs was more strongly inhibited by carmustine than was the growth of tumors isolated from monoculture constructs (Fig. 8C). This occurred because co-culture with macrophages significantly enhanced tumor cell growth and made chemotherapy more effective in these cells. The third experiment examined the effects of AS1517499 and BLZ945 in co-cultured glioblastoma-macrophage constructs (Fig. 8D). Tumor growth was hindered by BLZ945 but not by AS1517499, although both drugs downregulated GBM markers involved in angiogenesis, tumor immunity, and ECM remodeling [56].

GBM-on-a-chip constructs with patient-derived tumor cells were used to evaluate the patient-specific response to concurrent chemoradiation therapy (CCRT) with TMZ. As expected, each GBM-on-a-chip showed different survival to a single fraction of CCRT (15 Gy) with 950 μM TMZ and they could be separated into groups. A subsequent long-term follow up was performed in three constructs that received multiple fractions of CCRT (3 Gy) with 250 μM TMZ. Only cells from one construct displayed a complete loss of metabolic activity. The other two constructs showed a partial loss in their metabolic activity but regained full activity after 20 days of culture. These experiments clearly showed that differences exist between patients and they confirmed the usefulness of this platform for evaluating the best treatment for personalized medicine [72].

These results confirm that 3D models are better for pharmaceutical testing because they display a response that is remarkably similar to that displayed by the *in vivo* tumors. Furthermore, cancer cells in 3D structures show a higher resistance to different treatments compared to cells

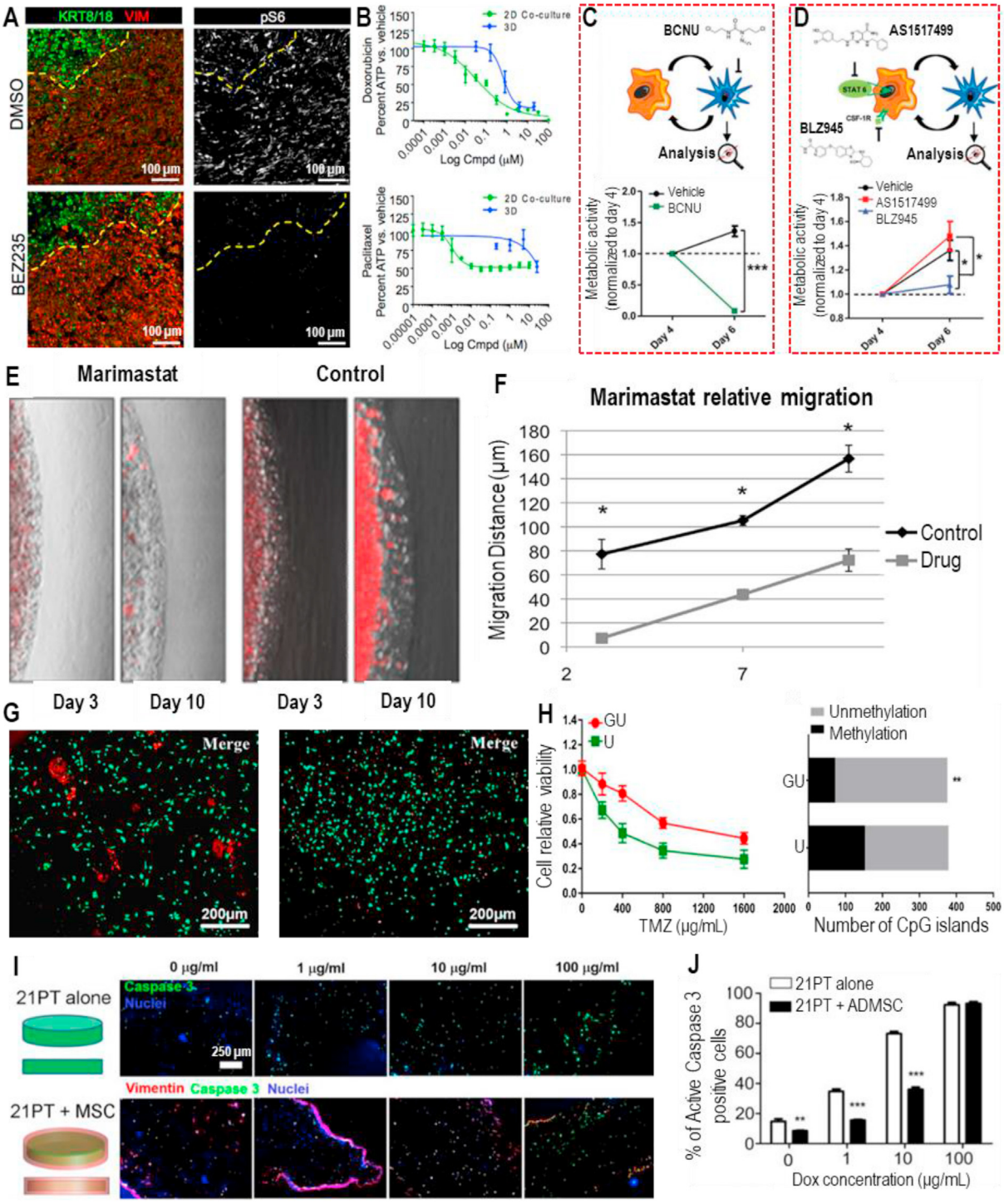

(caption on next page)

Fig. 8. Application of 3D bioprinted tumor models in pharmacological assessment. (A) Representative immunofluorescence images of lymphoblastoid bioprinted tissues treated with vehicle (dimethyl sulfoxide; DMSO) or BEZ235, an inhibitor of phosphatidylinositol 3-kinase (PI3K)/mammalian target of rapamycin (mTOR). Cells were stained for vimentin (VIM), cytokeratin 8/18 (KRT8/18), and phospho-S6 ribosomal protein (pS6). (Scale bars: 100 μm). (B) Dose response curves for 3D bioprinted constructs consisting of breast cancer cells (MCF-7) and preadipocytes and comparison with 2D co-cultures with the same ratio of cells. An ATP utilization assay was used to assess the constructs and cells that were treated with doxorubicin or paclitaxel. Adapted from Ref. [34]. (C) Schematic representation (upper panel) of treatment of cocultured glioblastoma-macrophage constructs, consisting of mouse macrophages (RAW264.7) and mouse glioblastoma cells (GL261), with carmustine (BCNU). The lower panel shows the metabolic activity of GL261 cells after coculture with RAW264.7 cells for 4 days. After the 4 days of co-culture, the two cell types were separated and treated with vehicle or BCNU for 48 h. (D) Schematic representation (upper panel) of treatment of the cocultured RAW264.7/GL261 constructs with either AS1517499, an inhibitor of signal transducer and activator of transcription 6 (Stat6), or BLZ945, an inhibitor of colony-stimulating factor 1 receptor (Csf-1r). The lower panel shows the metabolic activity of the GL261 cells after coculture with RAW264.7 at day 4 and 48 h after separation. During the co-culture period, cells received the treatments at days 1 and 3. Adapted from Ref. [56]. (E) Metastasis-on-a-chip device for examining the effects of Marimastat on migration of human colon carcinoma cells (HCT-116). Marimastat prevented the outward growth of aggregates from the 3D HCT-116 tumor constructs when compared with the untreated controls. (F) Quantification of the migration of HCT116 cells following treatment with or without Marimastat. Adapted from Ref. [54]. (G) Live/Dead staining of glioma cells (U118) harvested from hydrogel microfibers consisting of a shell-glioma stem cell GSC23/core-glioma cell line U118 (G/U) or a shell/core-U118 (U) after temozolomide (TMZ) treatment. (H) U118 cell viability after treatment with TMZ, normalized to an OD value of 0 μg mL-1 TMZ; the methylation rate of the MGMT promoter was lower in the G/U hydrogel microfibers than in the U hydrogel microfibers. Adapted from Ref. [84]. (I) Representative immunofluorescent staining for vimentin, cleaved caspase-3, and nuclei in human epidermal receptor 2 positive primary breast cancer cells (21 PT) and adipose-derived mesenchymal stem/stromal cells (ADMSCs) within bioprinted constructs. The cell constructs were cultured for 21 days and then treated with doxorubicin (DOX) for three days. (Scale bar: 250 μm). (J) Percentage of cells that showed positive staining for cleaved caspase-3, an apoptosis marker, based on the immunofluorescence staining analysis. Adapted from Ref. [63].

cultured in monolayers, and their response varies according to the presence of other cell types. These findings demonstrate the utility of these models for personalized medicine and drug discovery.

4.3.3. Ovarian and cervical cancer

The typical course of treatment for ovarian and cervical cancers involves the use of taxanes (paclitaxel) and platinum agents (carboplatin). In some models, combination regimens have been tested to determine whether a synergistic effect occurs.

HeLa cells have shown an enhanced chemoresistance to paclitaxel in 3D bioprinted constructs compared to the same cell line in 2D culture [89]. The EMT from 3D bioprinted HeLa cells induced by TGF-β was also dose-dependently inhibited by treatment with disulfiram and C19 (an EMT pathway inhibitor) [85].

In the case of ovarian cancer, 3D bioprinted OVCAR5 cells were used to test combination regimens that included photodynamic therapy (PDT), which sensitizes ovarian cancer cells to chemotherapy and targeted biological therapy. The experiments confirmed that PDT works in synergy with carboplatin in a sequence-dependent manner [95]. In this case, a cancerous process that is induced by a specific molecule can be reversed when adequate therapeutic agents are applied. Some combination regimens were also deemed to work better when they were applied in a defined sequential manner.

4.3.4. Other cancer models

Different types of cancer require different courses of treatment. Some chemotherapeutic agents work for several cancers and have been tested in several models. However, the use of immunomodulatory agents, such as monoclonal antibodies, requires the correct choice of therapeutic target. The use of *in vitro* models is also important for comparing different treatments to determine which one shows the best response.

HepG2 cells in a 3D bioprinted liver tumor construct showed higher resistance to 5-FU and mitomycin alone compared with cells in 2D monolayers, and the effect was partially reversed by the treatment with both drugs in combination [51]. This finding confirmed a synergistic effect of both drugs when used together.

A metastasis-on-a-chip platform was used to screen the effect of marimastat and 5-FU, which have different mechanisms of action, on a colon cancer model comprising Int-407 intestine epithelial cells and HCT-116 colon cancer cells. Marimastat was able to prevent outward growth of HCT-116 cells from the 3D gut constructs (Fig. 8E&F), while 5-FU caused a dose-dependent decrease in cell metabolism [54].

A previously mentioned pulmonary cancer model that included growth factors within the hydrogel was also used to test its feasibility for drug screening. This experiment took advantage of the vascularization of this tumor model, and drugs were delivered through the built-in vessel. The drugs were two immunotoxins designed with the same toxin fragments, but aimed at different targets. EGF4KDEL, which targets EGFR-overexpressing A549 cells, inhibited tumor cell growth and migration, whereas CD22KDEL, the off-target control, had no visible effect on A549 cell growth and migration. Consistent with other cancer models, cells in the 3D construct had a better resistance to these treatments than did cells growing in 2D monolayers [61].

The combination of 3D bioprinting, co-culture, and microfluidics has proven to be useful for creating realistic tumor models. One microfluidic chip system utilized a hepatoma model designed to test the monoclonal antibody Metuzumab. The microfluidic chip, which consisted of two channels interconnected by a trapezoidal microstructure array, was inoculated with HUVEC cells in one channel and hepatoma (SMMC-7721) spheroids in the other. Metuzumab was applied at different concentrations, but only the highest concentration affected the hepatoma spheroids in the microchips. The addition of peripheral blood mononuclear cells (PBMCs, consisting of lymphocytes and monocytes) to the model increased the antibody-dependent cell-mediated cytotoxicity with growing concentrations of Metuzumab. In addition, the expression of MMP2 and MMP9 was hindered only when PBMCs were present [79].

Gemcitabine was tested as a six-day treatment in a pancreatic ductal adenocarcinoma model consisting of patient-derived cancer cells, PSCs, and HUVECs. The cancer cells showed a dose-dependent cell death response with this treatment, as confirmed by immunofluorescence [34].

These models have been useful for different pharmaceutical purposes. Some have been used to test the specificity of immunomodulatory agents, and have confirmed their value for assessing if, for example, a monoclonal antibody will effectively discriminate between cancer cells and healthy cells. Other models confirmed that the 3D structure of bioprinted constructs affects the response to therapeutic agents and have been useful for defining clinically relevant doses.

5. Conclusions and perspectives

Cancer research has been greatly advanced by the development of 3D bioprinting, thanks to the fabrication of tumor models that improve the recapitulation of the tumor microenvironment. The types of solid tumors that have been modeled include breast, glioblastoma, ovarian, cervical, lung, colon, oral, pancreatic, and hepatoma cancers. Bioprinted tumors have integrated one or more of the components present in the TME, ranging from stromal and immune cells to vasculature and growth factors. Among the various bioprinting platforms, extrusion continues to be the most cost-effective and reliable for generating a relevant tumor microarchitecture with a high cell viability. When combined with the use of sacrificial hydrogels, extrusion bioprinting has been advantageous for creating pre-engineered micro vessels for the development of vascular

networks. However, the correct extrusion of bioinks relies on rheological tests of the hydrogels as prepolymers to assess their viscosity and elasticity and to confirm their printability. These tests, in turn, have identified combinations of different hydrogels that are practical for tuning the matrix stiffness, which then allows proper cell organization within the hydrogel.

Tumor model complexity has also increased both in structure and in components thanks to 3D printing. The different structures generated by 3D bioprinting have gone from microbeads and fibers to co-extruded fibers, which subsequently became grids and then multilayered grids. Sandwich structures, cylinders, discs, cubes, honeycombs, and even mini organs began to appear. The most recent examples have even combined 3D bioprinting with microfluidics to achieve highly ordered and well-designed constructs. Superior complexity of the models has also been achieved by adding several cell types, starting with cancer cells, and then including a different cell type derived from normal epithelial cells, fibroblasts, MSCs, macrophages and endothelial cells, or even combinations of these. The most difficult part of modeling a tumor has been adding vasculature, which has been attempted either by bioprinting endothelial cells into the construct and letting them self-organize into vascular networks or by leaving empty channels that can later be inoculated with endothelial cells.

These bioprinted tumors have now been used for several purposes. Depending on their structural organization, constructs are first characterized mainly by immunofluorescence and qPCR to confirm cell survival and to validate typical gene and protein expressions that are characteristic of tumor cells. This assessment can also be made with cells grown in 2D monolayer or biopsies to compare phenotypes. Biomarkers related to ECM remodeling, cell adhesion, cytoskeletal organization, stemness, angiogenesis, multidrug resistance, and metastasis have also been measured by these techniques.

The most common applications of bioprinted tumors are focused on the study of tumor biology, and particularly on processes that control migration, invasion, metastasis, and interaction of tumor cells with auxiliary cells that belong to the stroma or the immune system. Bioprinted tumors have also been fabricated to evaluate vascularization and related processes, such as endothelial barrier permeation, intravasation, and extravasation. More importantly, these models have been used to study drug responses with current chemotherapeutics, radiotherapy, photodynamic therapy, targeted therapies, and combinations of all of these. Bioprinted tumors have demonstrated higher resistance to therapeutic treatments than cells cultured in monolayer, so they display results similar to the actual outcomes observed in cancer patients. Bioprinted tumor models have confirmed that the presence of other cell types changes the response of cancer cells to cancer treatments, thereby emphasizing the importance of understanding the TME and its components in the search for therapeutic targets and molecules.

The fabrication of engineered tumor models using immortalized cell lines has proven to be a valuable resource to enable cancer research and to assess anti-cancer drug efficacy. However, an urgent need also exists to facilitate the inclusion of patient-derived cells into the design and use of this models [146]. In general, obtaining patient-derived tumor material for preclinical and biological studies is difficult due to its scarcity, and this has largely precluded studies of tumor biology and drug screening using patient tumor samples [74]. In this regard, however, a growing research area is now using biopsy-derived tumor cell cultures to fabricate organoids that retain the tumor heterogeneity observed in the patient [33]. Other approaches have used cancer slice cultures to evaluate drug responses [147]. Bioprinted tumor models have started to include patient-derived cancer cells, thereby beginning to close the gap between bioprinting platforms and the fabrication of personalized tumor models for drug screening. The availability of personalized tumor models will help physicians to choose the best course of treatment and to consequently achieve the best outcome possible for each patient. Currently, only a few reports have examined the use of patient-derived cancer cells with bioprinting platforms [34,50,56,72], but several other approaches are being used to generate personalized models; these have been extensively reviewed elsewhere [146]. There is a remarkably great potential of patient-derived organoids in biomedical research. Patient-derived tumor organoids have been recognized as an excellent pre-clinical cancer model for drug discovery and testing [148,149]. Recent papers describe the use of describe the use of patient-derived organoids in the context of bioprinting of cancer models [33,34,150].

The bioprinting of cancer spheroids in fibroblast-laden matrices could be applied to shorten the incubation period of these *in vitro* tumor models. Upcoming models must also consider that the TME is dynamically evolving, so stimulus-responsive hydrogels should be designed that could provide controlled release of various growth factors. Furthermore, the bioink designs should consider the physical properties of the tissue to be modeled, so that stiffness and cell adhesion sites are sufficient and adequate for the tumor being represented. For this purpose, bioinks could be supplemented with other natural components of the ECM specific for each type of cancer. The combination of 3D bioprinting and microfluidics [151] could also be better exploited to create models that include several cell types found within a typical tumor, as well as cells that embody other organs than can be affected by the represented cancer. In addition, since current models typically include either stromal or immune cells, the next step would be to include both cell types in a vascularized construct that holds growth factors and other signaling molecules.

The current pace at which 3D bioprinting is advancing will soon allow us to create better and more realistic tumor models for a wide range of solid cancers, with the ultimate goal of creating advanced models that are truly representative of the *in vivo* traits of those cancers. This will allow the materialization of personalized medicine for drug screening and evaluation of best treatment choices. The 3D bioprinting platforms, combined with recent advances in tissue engineering, genomics, proteomics, biomaterials, and microfluidics, will allow the biofabrication of new and better *in vitro* tumor models.

Funding

The authors acknowledge funding and scholarships provided by CONACYT (Consejo Nacional de Ciencia y Tecnología). GTdS acknowledges the funding received from L'Oréal-UNESCO-CONACyT-AMC (National Fellowship for Women in Science, México) and UC-MEXUS. MMA and GTdS acknowledge funding provided from the Biocodex Foundation in México.

CRediT authorship contribution statement

Mónica Gabriela Sánchez-Salazar: Writing - original draft, Investigation, Visualization. **Mario Moisés Álvarez:** Project administration, Writing - review & editing, Conceptualization, Supervision, Funding acquisition. **G. Trujillo-de Santiago:** Project administration, Writing - review & editing, Conceptualization, Supervision, Funding acquisition.

Declaration of competing interest

The authors declare that they have no known competing financial interests or personal relationships that could have appeared to influence the work reported in this paper.

Acknowledgments

The authors deeply acknowledge the support provided by Dr. Anne-Sophie Mertgen for English writing assistance and proofreading this review, and Elena Rima for her assistance improving the figures.

References

[1] M. Breitenbach, J. Hoffmann, Editorial: cancer models, Front. Oncol. 8 (2018) 1–4.
[2] J.U. Menon, 3D tumor models for cancer drug discovery : current status and outlook, J. Mecidine Ther. 2 (2018) 1–2.
[3] S.A. Langhans, Three-dimensional in vitro cell culture models in drug discovery and drug repositioning, Front. Pharmacol. 9 (2018) 1–14.
[4] J.L. Albritton, J.S. Miller, 3D bioprinting : improving in vitro models of metastasis with heterogeneous tumor microenvironments, Dis. Model. Mech. 10 (2017) 3–14.
[5] I. Cornil, D. Theodorescu, S. Man, M. Herlyn, J. Jambrosic, R.S. Kerbel, Fibroblast cell interactions with human melanoma cells affect tumor cell growth as a function of tumor progression, Proc. Natl. Acad. Sci. Unit. States Am. 88 (1991) 6028–6032.
[6] S. Liu, Y.Y. Xie, B. Wang, Role and prospects of regenerative biomaterials in the repair of spinal cord injury, Neural Regen. Res. 14 (2019) 1352–1363.
[7] Y. Yuan, Y.-C. Jiang, C.-K. Sun, Q.-M. Chen, Role of the tumor microenvironment in tumor progression and the clinical applications (Review), Oncol. Rep. 35 (2016) 2499–2515.
[8] J.K. Mouw, G. Ou, V.M. Weaver, Extracellular matrix assembly: a multiscale deconstruction, Nat. Rev. Mol. Cell Biol. 15 (2014) 771–785.
[9] T. Rozario, D.W. DeSimone, The extracellular matrix in development and morphogenesis: a dynamic view, Dev. Biol. 341 (2010) 126–140.
[10] S. Nallanthighal, J.P. Heiserman, D.-J. Cheon, The role of the extracellular matrix in cancer stemness, Front. Cell Dev. Biol. 7 (2019) 1–14.
[11] C. Walker, E. Mojares, A. del Río Hernández, Role of extracellular matrix in development and cancer progression, Int. J. Mol. Sci. 19 (2018) 3028.
[12] D.A. Senthebane, T. Jonker, A. Rowe, N.E. Thomford, D. Munro, C. Dandara, et al., The role of tumor microenvironment in chemoresistance: 3D extracellular matrices as accomplices, Int. J. Mol. Sci. 19 (2018) 2861.
[13] F. Hillen, A.W. Griffioen, Tumour vascularization: sprouting angiogenesis and beyond, Canc. Metastasis Rev. 26 (2007) 489–502.
[14] D. Mouradov, C. Sloggett, R.N. Jorissen, C.G. Love, S. Li, A.W. Burgess, et al., Colorectal cancer cell lines are representative models of the main molecular subtypes of primary cancer, Canc. Res. 74 (2014) 3238–3247.
[15] J.-P. Gillet, S. Varma, M.M. Gottesman, The clinical relevance of cancer cell lines, J. Natl. Cancer Inst. 105 (2013) 452–458.
[16] R.E. McIntyre, S.J.A. Buczacki, M.J. Arends, D.J. Adams, Mouse models of colorectal cancer as preclinical models, Bioessays 37 (2015) 909–920.
[17] M. Herreros-Villanueva, E. Hijona, A. Cosme, L. Bujanda, Mouse models of pancreatic cancer, World J. Gastroenterol. 18 (2012) 1286–1294.
[18] J. Li, J. Mai, L. Hinkle, D. Lin, J. Zhang, X. Liu, et al., Tracking biodistribution of myeloid-derived cells in murine models of breast cancer, Genes 10 (2019) 297.
[19] A. Kellar, C. Egan, D. Morris, Preclinical murine models for lung cancer: clinical trial applications, BioMed Res. Int. 2015 (2015) 621324.
[20] R.L. Johnson, J.C. Fleet, Animal models of colorectal cancer, Canc. Metastasis Rev. 32 (2013) 39–61.
[21] A.M. Navale, Animal models OF CANCER : a review, Int. J. Pharma Sci. Res. 4 (2013) 19–28.
[22] M. Cekanova, K. Rathore, Animal models and therapeutic molecular targets of cancer: utility and limitations, Drug Des. Dev. Ther. 8 (2014) 1911–1922.
[23] I.W.Y. Mak, N. Evaniew, M. Ghert, Lost in translation: animal models and clinical trials in cancer treatment, Am. J. Transl. Res. 6 (2014) 114–118.
[24] J. Hoarau-Véchot, A. Rafii, C. Touboul, J. Pasquier, Halfway between 2D and animal models: are 3D cultures the ideal tool to study cancer-microenvironment interactions? Int. J. Mol. Sci. 19 (2018).
[25] L.C. Kimlin, G. Casagrande, V.M. Virador, In Vitro three-dimensional (3D) models in cancer research: an update, Mol. Carcinog. 52 (2011) 167–182.
[26] F. Di Modugno, C. Colosi, P. Trono, G. Antonacci, G. Ruocco, P. Nisticò, 3D models in the new era of immune oncology: focus on T cells, CAF and ECM, J. Exp. Clin. Canc. Res. 38 (2019) 117–130.
[27] M.E. Katt, A.L. Placone, A.D. Wong, Z.S. Xu, P.C. Searson, In vitro tumor models: advantages, disadvantages, variables, and selecting the right platform, Front. Bioeng. Biotechnol. 4 (2016) 12–25.
[28] H. Fan, U. Demirci, P. Chen, Emerging organoid models: leaping forward in cancer research, J. Hematol. Oncol. 4 (2019) 142–151.
[29] M. Young, K.R. Reed, Organoids as a model for colorectal cancer, Curr. Colorectal Cancer Rep. 12 (2016) 281–287.
[30] H. Clevers, D.A. Tuveson, Organoid models for cancer, Annu. Rev. Cell Biol. 3 (2019) 234.
[31] K. Halfter, B. Mayer, Bringing 3D tumor models to the clinic – predictive value for personalized medicine, Biotechnol. J. 12 (2017) 1–16.
[32] E.L.S. Fong, T.B. Toh, H. Yu, E.K.-H. Chow, 3D culture as a clinically relevant model for personalized medicine, SLAS Technol 22 (2017) 245–253.
[33] E. Maloney, C. Clark, H. Sivakumar, K. Yoo, J. Aleman, S.A.P. Rajan, et al., Immersion bioprinting of tumor organoids in multi-well plates for increasing chemotherapy screening throughput, Micromachines 11 (2020) 208.
[34] E.M. Langer, B.L. Allen-Petersen, S.M. King, N.D. Kendsersky, M.A. Turnidge, G.M. Kuziel, et al., Modeling tumor phenotypes in vitro with three-dimensional bioprinting, Cell Rep. 26 (2019) 608–623.
[35] T.E. Yankeelov, N. Atuegwu, D. Hormuth, J.A. Weis, S.L. Barnes, M.I. Miga, et al., Clinically relevant modeling of tumor growth and treatment response, Sci. Transl. Med. 5 (2013) 187ps9.
[36] D. Lv, Z. Hu, L. Lu, H. Lu, X. Xu, Three-dimensional cell culture: a powerful tool in tumor research and drug discovery, Oncol. Lett. 14 (2017) 6999–7010.
[37] E. Sano, C. Mori, Y. Nashimoto, R. Yokokawa, H. Kotera, Y.S. Torisawa, Engineering of vascularized 3D cell constructs to model cellular interactions through a vascular network, Biomicrofluidics 12 (2018) 1–9.
[38] F.A. Auger, L. Gibot, D. Lacroix, The pivotal role of vascularization in tissue engineering, Annu. Rev. Biomed. Eng. 15 (2013) 177–200.
[39] S.V. Murphy, A. Atala, 3D bioprinting of tissues and organs, Nat. Biotechnol. 32 (2014) 773–785.
[40] A. Munaz, R.K. Vadivelu, St John J, M. Barton, H. Kamble, N.-T. Nguyen, Three-dimensional printing of biological matters, J. Sci. Adv. Mater. Devices 1 (2016) 1–17.
[41] Ž.P. Kacarevic, P.M. Rider, S. Alkildani, S. Retnasingh, R. Smeets, O. Jung, et al., An introduction to 3D bioprinting: possibilities, challenges and future aspects, Materials 11 (2018) 2199–2220.
[42] I. Matai, G. Kaur, A. Seyedsalehi, A. Mcclinton, C.T. Laurencin, Progress in 3D bioprinting technology for tissue/organ regenerative engineering, Biomaterials 226 (2020) 119536.
[43] D. Sundaramurthi, S. Rauf, C.A.E. Hauser, 3D bioprinting technology for regenerative medicine applications, Int. J. Bioprinting 2 (2016) 117–135.
[44] H. Tseng, J.A. Gage, T. Shen, W.L. Haisler, S.K. Neeley, S. Shiao, et al., A spheroid toxicity assay using magnetic 3D bioprinting and real-time mobile device-based imaging, Sci. Rep. 5 (2015) 1–11.
[45] H. Tseng, J.A. Gage, W.L. Haisler, S.K. Neeley, T. Shen, C. Hebel, et al., A high-throughput in vitro ring assay for vasoactivity using magnetic 3D bioprinting, Sci. Rep. 6 (2016) 1–8.
[46] D.A. Bowser, M.J. Moore, Biofabrication of neural microphysiological systems using magnetic spheroid bioprinting, Biofabrication 12 (2019).
[47] J.M. Lee, S.L. Sing, M. Zhou, W.Y. Yeong, 3D bioprinting processes: a perspective on classification and terminology, Int. J. Bioprinting 4 (2018) 1–10.
[48] J. Li, M. Chen, X. Fan, H. Zhou, Recent advances in bioprinting techniques: approaches, applications and future prospects, J. Transl. Med. 14 (2016) 1–15.
[49] X. Dai, C. Ma, Q. Lan, T. Xu, 3D bioprinted glioma stem cells for brain tumor model and applications of drug susceptibility, Biofabrication 8 (2016), 045005.
[50] X. Dai, L. Liu, J. Ouyang, X. Li, X. Zhang, Q. Lan, et al., Coaxial 3D bioprinting of self-assembled multicellular heterogeneous tumor fibers, Sci. Rep. 7 (2017) 1457.
[51] X. Wang, X. Zhao, X. Zhou, C. Liu, A 3D bioprinting liver tumor model for drug screening, World J. Pharm. Pharmaceut. Sci. 5 (2016) 196–213.
[52] D.M. Kingsley, C.L. Roberge, A. Rudkouskaya, D.E. Faulkner, M. Barroso, X. Intes, et al., Laser-based 3D bioprinting for spatial and size control of tumor spheroids and embryoid bodies, Acta Biomater. 95 (2019) 357–370.
[53] X. Wang, X. Zhang, X. Dai, X. Wang, X. Li, J. Diao, et al., Tumor-like lung cancer model based on 3D bioprinting, 3 Biotech 8 (2018) 501.
[54] A. Skardal, M. Devarasetty, S. Forsythe, A. Atala, S. Soker, A reductionist metastasis-on-a-chip platform for in vitro tumor progression modeling and drug screening, Biotechnol. Bioeng. 109 (2016) 1–13.
[55] X. Wang, X. Dai, X. Zhang, C. Ma, X. Li, T. Xu, et al., 3D bioprinted glioma cell-laden scaffolds enriching glioma stem cells via epithelial – mesenchymal transition, J. Biomed. Mater. Res. 107 (2018) 383–391.
[56] M.A. Heinrich, R. Bansal, T. Lammers, Y.S. Zhang, R.M. Schiffelers, J. Prakash, 3D-Bioprinted mini-brain : a glioblastoma model to study cellular interactions and therapeutics, Adv. Mater. 31 (2019) 1806590.
[57] T. Jiang, J.G. Munguia-Lopez, S. Flores-Torres, J. Grant, S. Vijayakumar, A De Leon-Rodriguez, et al., Directing the self-assembly of tumour spheroids by bioprinting cellular heterogeneous models within alginate/gelatin hydrogels, Sci. Rep. 7 (2017) 1–9.
[58] J.M. Grolman, D. Zhang, A.M. Smith, J.S. Moore, K.A. Kilian, Rapid 3D extrusion of synthetic tumor microenvironments, Adv. Mater. 27 (2015) 5512–5517.
[59] X. Wang, X. Li, X. Dai, X. Zhang, J. Zhang, T. Xu, et al., Bioprinting of glioma stem cells improves their endotheliogenic potential, Colloids Surf. B Biointerfaces 171 (2018) 629–637.
[60] C. Lee, E. Abelseth, L. de la Vega, S.M. Willerth, Bioprinting a novel glioblastoma tumor model using a fibrin-based bioink for drug screening, Mater. Today Chem. 12 (2019) 78–84.
[61] F. Meng, C.M. Meyer, D. Joung, D.A. Vallera, M.C. McAlpine, A. Panoskaltsis-Mortari, 3D bioprinted in vitro metastatic models via reconstruction of tumor microenvironments, Adv. Mater. 31 (2019) 1–10.
[62] X. Zhou, W. Zhu, M. Nowicki, S. Miao, H. Cui, B. Holmes, et al., 3D bioprinting a cell-laden bone matrix for breast cancer metastasis study, ACS Appl. Mater. Interfaces 8 (2016) 30017–30026.
[63] Y. Wang, W. Shi, M. Kuss, S. Mirza, D. Qi, A. Krasnoslobodtsev, et al., 3D bioprinting of breast cancer models for drug resistance study, ACS Biomater. Sci. Eng. 4 (2018) 4401–4411.
[64] N. Peela, F.S. Sam, W. Christenson, D. Truong, A.W. Watson, G. Mouneimne, et al., A three dimensional micropatterned tumor model for breast cancer cell migration studies, Biomaterials 81 (2016) 72–83.
[65] W. Zhu, B. Holmes, R.I. Glazer, L.G. Zhang, 3D printed nanocomposite matrix for the study of breast cancer bone metastasis, Nanomed. Nanotechnol. Biol. Med. 12 (2016) 6979.
[66] P. Soman, J.A. Kelber, J.W. Lee, T.N. Wright, K.S. Vecchio, R.L. Klemke, et al., Cancer cell migration within 3D layer-by-layer microfabricated photocrosslinked PEG scaffolds with tunable stiffness, Biomaterials 33 (2012) 7064–7070.
[67] T.Q. Huang, X. Qu, J. Liu, S. Chen, 3D printing of biomimetic microstructures for cancer cell migration, Biomed. Microdevices 16 (2014) 127–132.
[68] J.A. Reid, X.-L. Palmer, P.A. Mollica, N. Northam, P.C. Sachs, R.D. Bruno, A 3D bioprinter platform for mechanistic analysis of tumoroids and chimeric mammary organoids, Sci. Rep. 9 (2019) 7466.

[69] T. Almela, S. Al-Sahaf, I.M. Brook, K. Khoshroo, M. Rasoulianboroujeni, F. Fahimipour, et al., 3D printed tissue engineered model for bone invasion of oral cancer, Tissue Cell 52 (2018) 71–77.

[70] S. Swaminathan, Q. Hamid, W. Sun, A.M. Clyne, Bioprinting of 3D breast epithelial spheroids for human cancer models, Biofabrication 11 (2019), 025003.

[71] F. Xu, J. Celli, I. Rizvi, S. Moon, T. Hasan, U. Demirci, A three-dimensional in vitro ovarian cancer coculture model using a high-throughput cell patterning platform, Biotechnol. J. 6 (2011) 204–212.

[72] H.-G. Yi, Y.H. Jeong, Y. Kim, Y. Choi, H.E. Moon, S.H. Park, et al., A bioprinted human-glioblastoma-on-a-chip for the identification of patient-specific responses to chemoradiotherapy, Nat. Biomed. Eng. 3 (2019) 509–519.

[73] Y.S. Zhang, K. Yue, J. Aleman, K.M. Moghaddam, S.M. Bakht, J. Yang, et al., 3D bioprinting for tissue and organ fabrication, Ann. Biomed. Eng. 45 (2016) 148–163.

[74] D.F. Duarte Campos, A. Bonnin Marquez, C. O'Seanain, H. Fischer, A. Blaeser, M. Vogt, et al., Exploring cancer cell behavior in vitro in three-dimensional multicellular bioprintable collagen-based hydrogels, Cancers vol. 11 (2019).

[75] M.A. Hermida, J.D. Kumar, D. Schwarz, K.G. Laverty, A. Di Bartolo, M. Ardron, et al., Three dimensional in vitro models of cancer : bioprinting multilineage glioblastoma models, Adv. Biol. Regul. 75 (2020) 100658.

[76] I.K. Zervantonakis, S.K. Hughes-alford, J.L. Charest, J.S. Condeelis, Three-dimensional microfluidic model for tumor cell intravasation and endothelial barrier function, Proc. Natl. Acad. Sci. Unit. States Am. 109 (2012) 13515–13520.

[77] B. Holmes, W. Zhu, L.G. Zhang, Development of a novel 3D bioprinted in vitro nano bone model for breast cancer bone metastasis study, in: Materials Research Society Symposium Proceedings, 2014, pp. 1–6.

[78] S.M. King, V. Gorgen, S.C. Presnell, D.G. Nguyen, B.R. Shepherd, N. Ridge, et al., Development of 3D bioprinted human breast cancer for in vitro screening of therapeutics targeted against cancer progression, in: Tissue Applications and Systems Engineering Groups, 2013, p. 6275.

[79] Y. Li, T. Zhang, Y. Pang, L. Li, Z.N. Chen, W. Sun, 3D bioprinting of hepatoma cells and application with microfluidics for pharmacodynamic test of Metuzumab, Biofabrication 11 (2019).

[80] M. Jafarkhani, Z. Salehi, A. Aidun, M.A. Shokrgozar, Bioprinting in vascularization strategies, Iran. Biomed. J. 23 (2019) 9–20.

[81] T.G. Papaioannou, D. Manolesou, E. Dimakakos, G. Tsoucalas, M. Vavuranakis, D. Tousoulis, 3D bioprinting methods and Techniques : applications on artificial blood vessel fabrication, Acta Cardiol. Sin. 35 (2019) 284–289.

[82] B. Byambaa, N. Annabi, K. Yue, G. Trujillo-de Santiago, M.M. Alvarez, W. Jia, et al., Bioprinted osteogenic and vasculogenic patterns for engineering 3D bone tissue, Adv. Healthc. Mater. 6 (2017) 1–15.

[83] G. Trujillo-De Santiago, M.M. Alvarez, M. Samandari, G. Prakash, G. Chandrabhatla, P.I. Rellstab-Sánchez, et al., Chaotic printing: using chaos to fabricate densely packed micro- and nanostructures at high resolution and speed, Mater. Horizons 5 (2018) 813–822.

[84] X. Wang, X. Li, X. Dai, X. Zhang, J. Zhang, T. Xu, et al., Coaxial extrusion bioprinted shell-core hydrogel microfibers mimic glioma microenvironment and enhance the drug resistance of cancer cells, Colloids Surf. B Biointerfaces 171 (2018) 291–299.

[85] Y. Pang, S.S. Mao, R. Yao, J.Y. He, Z.Z. Zhou, L. Feng, et al., TGF-β induced epithelial-mesenchymal transition in advanced cervical tumor model by 3D printing, Biofabrication 10 (2018), 044102.

[86] V.K. Lee, G. Dai, H. Zou, S.S. Yoo, Generation of 3-D glioblastoma-vascular niche using 3-D bioprinting, in: 41st Annual Northeast Biomedical Engineering Conference, NEBEC, 2015, pp. 3–4.

[87] E.A. Kiyotake, A.W. Douglas, E.E. Thomas, S.L. Nimmo, M.S. Detamore, Development and quantitative characterization of the precursor rheology of hyaluronic acid hydrogels for bioprinting, Acta Biomater. 95 (2019) 176–187.

[88] J. Lewicki, J. Bergman, C. Kerins, O. Hermanson, Optimization of 3D bioprinting of human neuroblastoma cells using sodium alginate hydrogel, Bioprinting 16 (2019), e00053.

[89] Y. Zhao, R. Yao, L. Ouyang, H. Ding, T. Zhang, K. Zhang, et al., Three-dimensional printing of Hela cells for cervical tumor model in vitro, Biofabrication 6 (2014), 035001.

[90] S. Han, S. Kim, Z. Chen, H.K. Shin, S.Y. Lee, H.E. Moon, et al., 3D bioprinted vascularized tumour for drug testing, Int. J. Mol. Sci. 21 (2020) 1–14.

[91] S.K. Schmidt, R. Schmid, A. Arkudas, A. Kengelbach-Weigand, A.K. Bosserho, Tumor cells develop defined cellular phenotypes after 3D-bioprinting in different bioinks, Cells 8 (2019) 1295.

[92] X. Xu, L.A. Gurski, C. Zhang, D.A. Harrington, M.C. Farach-Carson, X. Jia, Recreating the tumor microenvironment in a bilayer, hyaluronic acid hydrogel construct for the growth of prostate cancer spheroids, Biomaterials 33 (2012) 9049–9060.

[93] P.A. Mollica, E.N. Booth-Creech, J.A. Reid, M. Zamponi, S.M. Sullivan, X.L. Palmer, et al., 3D bioprinted mammary organoids and tumoroids in human mammary derived ECM hydrogels, Acta Biomater. 95 (2019) 201–213.

[94] K. Hölzl, S. Lin, L. Tytgat, S. Van Vlierberghe, L. Gu, A. Ovsianikov, Bioink properties before, during and after 3D bioprinting, Biofabrication 8 (2016), 032002.

[95] I. Rizvi, J.P. Celli, F. Xu, C.L. Evans, A.O. Abu-Yousif, A. Muzikansky, et al., Biologically-relevant 3D tumor arrays: treatment response and the importance of stromal partners. Optical Methods for Tumor Treatment and Detection: Mechanisms and Techniques in Photodynamic Therapy XX, 2011, pp. 1–14.

[96] K. Ling, G. Huang, J. Liu, X. Zhang, Y. Ma, T. Lu, et al., Bioprinting-based high-throughput fabrication of three-dimensional MCF-7 human breast cancer cellular spheroids, Engineering 1 (2015) 269–274.

[97] A. Campbell, J.E. Mohl, D.A. Gutierrez, A. Varela-Ramirez, T. Boland, Thermal bioprinting causes ample alterations of expression of LUCAT1, IL6, CCL26, and NRN1L genes and massive phosphorylation of critical oncogenic drug resistance pathways in breast cancer cells, Front. Bioeng. Biotechnol. 8 (2020) 1–15.

[98] T. Jiang, J.G. Munguia-Lopez, K. Gu, M.M. Bavoux, S. Flores-Torres, J. Kort-Mascort, et al., Engineering bioprintable alginate/gelatin composite hydrogels with tunable mechanical and cell adhesive properties to modulate tumor spheroid growth kinetics, Biofabrication 12 (2020) 32.

[99] D. Hakobyan, C. Médina, N. Dusserre, M.-L. Stachowicz, C. Handschin, J.-C. Fricain, et al., Laser-assisted 3D bioprinting of exocrine pancreas spheroid models for cancer initiation study, Biofabrication 12 (2020), 035001.

[100] J.M. Lee, W.L. Ng, W.Y. Yeong, Resolution and shape in bioprinting: strategizing towards complex tissue and organ printing, Appl. Phys. Rev. (2019) 6, https://doi.org/10.1063/1.5053909 [Internet], Available from:.

[101] R. Utama, L. Atapattu, A. O'Mahony, C. Fife, J. Baek, T. Allard, et al., Precise, High-Throughput Production of Multicellular Spheroids with a Bespoke 3D Bioprinter, vols. 1–26, 2020.

[102] D.F. Duarte Campos, C.D. Lindsay, J.G. Roth, B.L. LeSavage, A.J. Seymour, B.A. Krajina, et al., Bioprinting cell- and spheroid-laden protein-engineered hydrogels as tissue-on-chip platforms, Front. Bioeng. Biotechnol. 8 (2020) 1–13.

[103] S. Samavedi, N. Joy, 3D printing for the development of in vitro cancer models, Curr. Opin. Biomed. Eng. 2 (2017) 35–42.

[104] T. Courau, J. Bonnereau, J. Chicoteau, H. Bottois, R. Remark, L.A. Miranda, et al., Cocultures of human colorectal tumor spheroids with immune cells reveal the therapeutic potential of MICA/B and NKG2A targeting for cancer treatment, J. Immunother. Cancer 7 (2019) 74.

[105] T. Liu, Q. Liu, I. Anaya, D. Huang, W. Kong, L.S. Mille, et al., Investigating lymphangiogenesis in a sacrificially bioprinted volumetric model of breast tumor tissue, Methods 1 (2020).

[106] X. Jin, P. Mu, Targeting breast cancer metastasis. Breast cancer basic, Clin. Res. 9 (2015) 23–34.

[107] D.M. van Pel, K. Harada, D. Song, C.C. Naus, W.C. Sin, Modelling glioma invasion using 3D bioprinting and scaffold-free 3D culture, J. Cell Commun. Signal. 12 (2018) 723–730.

[108] J.S. Jeon, I.K. Zervantonakis, S. Chung, R.D. Kamm, J.L. Charest, In Vitro model of tumor cell extravasation, PloS One 8 (2013), e56910.

[109] P. Agarwal, H. Wang, M. Sun, J. Xu, S. Zhao, Z. Liu, et al., Microfluidics enabled bottom-up engineering of 3D vascularized tumor for drug discovery, ACS Nano 11 (2017) 6691–6702.

[110] H. Ide, M. Okada, K. Sakihama, T. Katsuki, Y. Minamishima, "Transformation" of human endothelial cells by SV40 virions, Microbiol. Immunol. 32 (1988) 45–55.

[111] F. Leonard, B. Godin, 3D in vitro model for breast cancer research using magnetic levitation and bioprinting method, Methods Mol. Biol. 1406 (2016) 239–251.

[112] S. Chaji, J. Al-Saleh, C.T. Gomillion, Bioprinted three-dimensional cell-laden hydrogels to evaluate adipocyte-breast cancer cell interactions, Gels 6 (2020).

[113] C. Colosi, S.R. Shin, V. Manoharan, S. Massa, M. Costantini, A. Barbetta, et al., Microfluidic bioprinting of heterogeneous 3D tissue constructs using low-viscosity bioink, Adv. Mater. 28 (2016) 677–684a.

[114] B. Gantenbein-Ritter, C.M. Sprecher, S. Chan, S. Illien-Jünger, S. Grad, Confocal imaging protocols for live/dead staining in three-dimensional carriers, in: mammalian cell viability. methods in molecular biology, 2011, pp. 127–140.

[115] T.L. Riss, R.A. Moravec, A.L. Niles, S. Duellman, H.A. Benink, T.J. Worzella, et al., Cell viability assays, in: G. Sittampala, A. Grossman, K. Brimacombe (Eds.), Assay Guidance Manual, Eli Lilly & Company and the National Center for Advancing Translational Sciences, 2016, p. 28, 2004.

[116] S.N. Rampersad, Multiple applications of alamar blue as an indicator of metabolic function and cellular health in cell viability bioassays, Sensors 12 (2012) 12347–12360.

[117] M. Jeppesen, G. Hagel, A. Glenthoj, B. Vainer, P. Ibsen, H. Harling, et al., Short-term spheroid culture of primary colorectal cancer cells as an in vitro model for personalizing cancer medicine, PloS One 12 (2017) 1–19.

[118] S. Cattin, L. Ramont, C. Rüegg, Characterization and in vivo validation of a three-dimensional multi-cellular culture model to study heterotypic interactions in colorectal cancer cell growth, invasion and metastasis, Front. Bioeng. Biotechnol. 6 (2018) 1–14.

[119] W. Zhu, X. Qu, J. Zhu, X. Ma, S. Patel, J. Liu, et al., Direct 3D bioprinting of prevascularized tissue constructs with complex microarchitecture, Biomaterials 124 (2017) 106–115.

[120] O. Candini, G. Grisendi, E.M. Foppiani, M. Brogli, B. Aramini, V. Masciale, et al., A novel 3D in vitro platform for pre-clinical investigations in drug testing, gene therapy, and immuno-oncology, Sci. Rep. 9 (2019) 7154.

[121] J. Neradil, R. Veselska, Nestin as a marker of cancer stem cells, Canc. Sci. 106 (2015) 803–811.

[122] Z. Li, CD133: a stem cell biomarker and beyond, Exp. Hematol. Oncol. 2 (2013) 17–24.

[123] Y. Itoh, H. Nagase, Matrix metalloproteinases in cancer, Essays Biochem. 38 (2002) 21–36.

[124] S. Sharma, F. Salehi, B.W. Scheithauer, F. Rotondo, L.V. Syro, K. Kovacs, Role of MGMT in tumor development, progression, diagnosis, treatment and prognosis, Anticancer Res. 29 (2009) 3759–3768.

[125] L. Zhang, S.-B. Ye, Z.-L. Li, G. Ma, S.-P. Chen, J. He, et al., Increased HIF-1alpha expression in tumor cells and lymphocytes of tumor microenvironments predicts unfavorable survival in esophageal squamous cell carcinoma patients, Int. J. Clin. Exp. Pathol. 7 (2014) 3887–3897.

[126] M. Zhang, T. Song, L. Yang, R. Chen, L. Wu, Z. Yang, et al., Nestin and CD133: valuable stem cell-specific markers for determining clinical outcome of glioma patients, J. Exp. Clin. Canc. Res. 27 (2008) 85–91.
[127] R. Goyal, S.K. Mathur, S. Gupta, R. Goyal, S. Kumar, A. Batra, et al., Immunohistochemical expression of glial fibrillary acidic protein and CAM5 . 2 in glial tumors and their role in differentiating glial tumors from metastatic tumors of central nervous system, J. Neorosciences Rural Pract. 6 (2015) 499–503.
[128] C.D. Katsetos, P. Dráber, M. Kavallaris, Targeting BIII-tubulin in glioblastoma multiforme: from cell biology and histopathology to cancer therapeutics, Anticancer Agents Med. Chem. 11 (2011) 719–728.
[129] F.G. Zhang J, M. Stevens, D. Bradshaw T, Temozolomide: mechanisms of action, repair and resistance, Curr. Mol. Pharmacol. 5 (2012) 102–114.
[130] D. Shaloam, P.B. Tchounwou, Cisplatin in cancer therapy: molecular mechanisms of action, Eur. J. Pharmacol. 740 (2014) 364–378.
[131] A.B. Fleming, W.M. Saltzman, Pharmacokinetics of the carmustine implant, Clin. Pharmacokinet. 41 (2002) 403–419.
[132] F. Yu, W. Bender, The mechanism of tamoxifen in breast cancer prevention. Breast Cancer Research, 2001.
[133] M. Ono, M. Kuwano, Molecular mechanisms of epidermal growth factor receptor (EGFR) activation and response to gefitinib and other EGFR-targeting drugs, Clin. Canc. Res. 12 (2006) 7242–7251.
[134] P.D. Ottewell, J.K. Woodward, D.V. Lefley, C.A. Evans, R.E. Coleman, I. Holen, Anticancer mechanisms of doxorubicin and zoledronic acid in breast cancer tumor growth in bone, Mol. Canc. Therapeut. 8 (2009) 2821–2832.
[135] P. De, J.C. Aske, N. Dey, RAC1 takes the lead in solid tumors, Cells 8 (2019) 382.
[136] C.F. Thorn, C. Oshiro, S. Marsh, T. Hernandez-Boussard, H. McLeod, T.E. Klein, et al., Doxorubicin pathways, Pharmacogenetics Genom. 21 (2011) 440–446.
[137] C. Le Tourneau, E. Raymond, Faivre S. Sunitinib, A novel tyrosine kinase inhibitor. A brief review of its therapeutic potential in the treatment of renal carcinoma and gastrointestinal stromal tumors (GIST), Therapeut. Clin. Risk Manag. 3 (2007) 341–348.
[138] B.A. Weaver, How Taxol/paclitaxel kills cancer cells, Mol. Biol. Cell 25 (2014) 2677–2681.
[139] N. Zhang, Y. Yin, S.J. Xu, W.S. Chen, 5-Fluorouracil: mechanisms of resistance and reversal strategies, Molecules 13 (2008) 1551–1569.
[140] M.M. Paz, X. Zhang, J. Lu, A. Holmgren, A new mechanism of action for the anticancer drug Mitomycin C: mechanism-based inhibition of thioredoxin reductase, Chem. Res. Toxicol. 25 (2012) 1502–1511.
[141] F. Feng, B. Wang, X. Sun, Y. Zhu, H. Tang, G. Nan, et al., Metuzumab enhanced chemosensitivity and apoptosis in non-small cell lung carcinoma, Canc. Biol. Ther. 18 (2017) 51–62.
[142] Q. Spillier, D. Vertommen, S. Ravez, R. Marteau, Q. Thémans, C. Corbet, et al., Anti-alcohol abuse drug disulfiram inhibits human PHGDH via disruption of its active tetrameric form through a specific cysteine oxidation, Sci. Rep. 9 (2019) 1–9.
[143] G.F. de Sousa, S.R. Wlodarczyk, G. Monteiro, Carboplatin: molecular mechanisms of action associated with chemoresistance, Brazilian J. Pharm. Sci. 50 (2014) 693–702.
[144] B.J. Stish, S. Oh, H. Chen, A.Z. Dudek, R.A. Kratzke, D.A. Vallera, Design and modification of EGF4KDEL 7Mut, a novel bispecific ligand-directed toxin, with decreased immunogenicity and potent anti-mesothelioma activity, Br. J. Canc. 101 (2009) 1114–1123.
[145] L. De Sousa Cavalcante, G. Monteiro, Gemcitabine: metabolism and molecular mechanisms of action, sensitivity and chemoresistance in pancreatic cancer, Eur. J. Pharmacol. 741 (2014) 8–16.
[146] L.J. Bray, D.W. Hutmacher, N. Bock, Addressing patient specificity in the engineering of tumor models, Front. Bioeng. Biotechnol. 7 (2019) 1–36.
[147] L.F. Horowitz, A.D. Rodriguez, Z. Dereli-Korkut, R. Lin, K. Castro, A.M. Mikheev, et al., Multiplexed drug testing of tumor slices using a microfluidic platform, npj Precis. Oncol. 4 (2020).
[148] F. Weeber, S.N. Ooft, K.K. Dijkstra, E.E. Voest, Tumor organoids as a pre-clinical cancer model for drug discovery, Cell Chem. Biol. 24 (2017) 1092–1100, https://doi.org/10.1016/j.chembiol.2017.06.012 [Internet], Available from:.
[149] S. Yin, R. Xi, A. Wu, S. Wang, Y. Li, C. Wang, et al., Patient-derived tumor-like cell clusters for drug testing in cancer therapy, Sci. Transl. Med. 12 (2020).
[150] M. Chadwick, C. Yang, L. Liu, C.M. Gamboa, K. Jara, H. Lee, et al., Rapid processing and drug evaluation in glioblastoma patient-derived organoid models with 4d bioprinted arrays, iScience vol. 23 (2020) 101365, https://doi.org/10.1016/j.isci.2020.101365 [Internet], Available from:.
[151] H. Zhao, Y. Chen, L. Shao, M. Xie, J. Nie, J. Qiu, et al., Airflow-assisted 3D bioprinting of human heterogeneous microspheroidal organoids with microfluidic nozzle, Small 14 (2018) 1–7.